arXiv:1208.2742v2 [cond-mat.mes-hall] 18 Aug 2012

Topological phases and Majorana Fermions in quantum wires: from magnetostatic to non-magnetic Floquet platforms

Andres A. Reynoso[1] and Diego Frustaglia[2]
[1]*Centre for Engineered Quantum Systems, School of Physics, The University of Sydney, NSW 2006, Australia*
[2]*Departamento de Física Aplicada II, Universidad de Sevilla, E-41012 Sevilla, Spain*

(Dated: August 21, 2012)

Quantum wires subject to the combined action of spin-orbit and Zeeman coupling in the presence of s-wave pairing potentials (superconducting proximity effect in semiconductors or superfluidity in cold atoms) are one of the most promising systems for the developing of topological phases hosting Majorana fermions. Other potential platforms can be obtained by applying appropriate transformations to the quantum-wire model. One example is the recent proposal by Kjaergaard et al. [Phys. Rev. B 85, 020503(R) (2012)], where an effective spin-orbit coupling is obtained in electronic systems subject to magnetic textures after applying a local spin-rotation mapping. Here, instead, we employ a *time-dependent* spin rotation that maps the standard magnetostatic model into a *non-magnetic* one where the spin-orbit coupling axis changes as a function of time. This represents a proposal for the development of a topological state of matter driven by external forces. From a practical viewpoint, though the scheme avoids the disadvantages of conjugating magnetism and superconductivity, the need of a high-frequency driving of spin-orbit coupling represents a technological challenge. We describe the basic properties of this Floquet system and show that in finite samples it hosts Floquet Majorana fermions at its edges despite the fact that the bulk Floquet quasienergies are gapless and that the Hamiltonian at each instant of time is a time-reversal symmetric operator. The exact mapping to the static system allows us to show that the localized Floquet Majorana fermions are robust to local perturbations, this result is found to be in agreement with numerical simulations fully performed in the time-dependent system.

PACS numbers: 03.65.Vf, 71.10.Pm, 73.21.Hb, 74.78.Na, 71.70.Ej, 05.30.Rt

I. INTRODUCTION

Experimental research in the field of hybrid systems involving spin-orbit coupling (SOC) and superconductivity is currently booming.[1–4] It has been predicted that systems based on topological insulators,[5] semiconducting quantum wires,[6,7] or Bose-Einstein condensates (BECs) in ultracold atoms,[8,9] can realize the topological superconducting phase (TSP) [which was theoretically predicted to appear in spinless p-wave paired fermions].[10] In particular the one-dimensional (1D) proposals that hosts unpaired Majorana fermions at its edges can be thought of a realization of Read and Green phase in 1D,[10] or of the Kitaev 1D model.[11] In these physical platforms the access to the TSP is achieved by breaking time-reversal (TR) symmetry with an additional magnetic field, the corresponding Zeeman energy must be larger than a critical value.

The virtue of the proposals using semiconducting spin-orbit coupled (SOC) samples in proximity to s-wave superconductors, is being practical schemes exploding the fact that an explicit p-wave superconductivity is not required to realize the TSP: as first reported for superfluid ultracold fermion atoms systems.[8] While because of the helical nature of the edge states in topological insulators the s-wave BCS pairing plays the role of a p-wave in spinless systems,[12] in semiconducting (ultracold atoms) systems it is the combination of an explicit spin-orbit interaction and the s-wave superconductivity (superfluidity/BEC) what gives access to the TSP for Zeeman energies above a critical value. In finite-size systems the success of any of those proposals would lead to an unprecedented breakthrough: the synthesization of the elusive Majorana fermions (MFs). Beyond the relevance for fundamental physics, such a finding—probably already realized—[2–4,13] would unveil a new set of technological possibilities: since space localized MFs are Ising anyons, their topological properties can be profited for applications in quantum information and quantum computation.[11,14–17]

In parallel, the growing interest in topological phases of matter has led to study them in non-equilibrium conditions. It has been shown, by using Floquet theory for dealing with time-periodic Hamiltonians, that topological phases can be realized including phases that have no analog in static systems.[18] For example, there has been several studies on graphene subject to electromagnetic radiation in the microwave-THz regime.[19–24] In the case of circular polarized radiation topological insulating properties arise that give rise to the existence of gapless edge states. Another interesting proposal is the Floquet topological insulator in semiconducting systems.[25] Moreover, 1D photonic bound states at the interface between two distinct Floquet topological phases have been predicted,[25] and detected.[26] Recently, in Ref. 9, localized Floquet Majorana fermions (FMFs) have been predicted to appear in cold-atom quantum wires due to periodical change of the chemical potential. Similarly, FMF 1D modes were recently predicted to appear at edges of a cold-atom superfluid 2D system in which the potential of the optical square lattice is periodically modulated.[27]

Our starting point here is the 1D model for a quantum wire in which spin-orbit coupling, s-wave pairing potential, and Zeeman interaction (all of them static and spatially uniform) coexist.[6] We intend to gain insight into alternative systems and mechanisms where a topological phase can emerge by applying unitary maps to the original model. This is achieved by choosing suitable transformations removing either the spin-orbit interaction or the Zeeman coupling from the original electronic Hamiltonian $\hat{H}_{0,\mathrm{e}}$. In the transformed system, while an interacting term is absent the remaining ones are modified. A physical system described by the transformed Hamiltonian can potentially share some topological properties of the original system.[28] The removal of the SOC term brings upon a successful example of this scheme,[29] allowing the derivation of the spin-orbit free topological platform reported in Ref. 30. We note that, for systems in which a magnetic field is required, it is also important knowing how to replace its effect with alternative schemes.[31–34] Here, inspired by concepts of nuclear magnetic resonance,[35] we report a novel topological platform for Floquet Majorana fermions found by removing the Zeeman term in the originally static Hamiltonian: a 1D quantum wire which is subject to a periodical driven SOC.

The proposed platform *does not require* any external magnetic field or proximity to magnetic materials. This avoids the difficulties of combining superconductivity and magnetism, where the Meissner effect could hinder the development of topological phases due to the subcritical magnetic screening in the quantum wire– see Eq.(5). This profit is counterpointed by the need of a periodical modulation of the SOC-axis that should not degrade the pairing potential. In spite of the technical difficulties this could imply, our proposal emerges as an original case study in the active field of topological phases in driven systems.[27,36]

We start by studying the Floquet quasienergy spectrum for an infinite quantum wire, finding a family of excitations forming a Dirac cone that becomes gapless at small wavenumber k only for a critical driving frequency Ω_c. We predict the value of the critical frequency by mapping the Floquet system to the static 1D topological superconductor system. The system here is ungapped in Floquet quasienergies when including solutions for all k. However, as pointed out by Kitagawa et al. in Ref. 18, topological properties can be present in such condition.

We also investigate the mean energies of the Floquet solutions, i.e., the expectation value of the Hamiltonian averaged over one driving period. At small k we find that the family of solutions in the quasienergy Dirac cone—closing at a finite quasienergy value—produces a Dirac cone in mean energy that closes at zero energy for the critical driving frequency.[37] Remarkably, in this system the topological phase can be distinguished from the trivial phase directly from the mean energy of the Floquet states at small k.

We further focus on a finite piece of wire, obtaining Floquet Majorana Fermions localized at its edges. This is shown both by using the mapping to the static system and by solving numerically the time dependent problem. The FMFs appear at a finite and well-defined quasienergy. Remarkable, the FMFs appear even though the Hamiltonian at each instant of time does not violates TR symmetry. However, because of the full period evolution, TR symmetry is violated and thus the system satisfies such necessary condition for the appearance of unpaired Majorana fermions. We have numerically explored periodical SOC excitations that do not violate TR symmetry, we find that the quasienergy spectrum appears double degenerated and the FMFs are not observed.

The finite quasienergy at which the FMFs appear is the same as that reported in Ref. 9 for one type of FMFs. We point out that, because such quasienergy is proportional to the driving frequency, the state has *zero* mean energy. Recently, in Ref. 38, Arimondo et al. suggested, with experimental support, that the statistics of the non-equilibrium populations of the Floquet states could be determined by Bose-Einstein (for bosons) or Fermi-Dirac (for fermions) distributions in the *mean-energy variable*. If that is the case the mean energy would play the role of the energy in static systems. Similar conclusions are theoretically drawn in some limits for a Floquet system in contact with a thermal bath.[39] These results would imply that there might be some regimes in which the FMFs can be the highest mean energy occupied Floquet states because the FMFs have zero mean energy which is aligned with the chemical potential.

Finally, by working entirely in the time-dependent system we numerically verify the robustness of the obtained FMFs by showing that they arise in the presence of static local disorder. This is expected by virtue of our *exact mapping* to the static system of Ref. 6. In the presence of such disorder we investigate several types of interfaces involving the Floquet topological system.

The paper is organized as follows. In Sec. II we outline the derivation of the non-magnetic Floquet platform. In Sec. III we explore its properties for both infinite and finite samples, identifying the presence of Floquet Majorana fermions. Further discussion and conclusions are presented in Sec. IV.

II. DERIVATION OF TWO ALTERNATIVE TOPOLOGICAL PLATFORMS

We start by introducing the quantum-wire platform in which the interactions are constant as a function of time and position. In the absence of superconductivity, the electrons in the wire follow the Hamiltonian

$$\hat{H}_{0,\mathrm{e}} = \hat{H}_{\mathrm{kin}} + \hat{H}_{\mathrm{Z}} + \hat{H}_{\mathrm{so}}, \tag{1a}$$

$$\hat{H}_{\mathrm{kin}} = \frac{p_x^2}{2m^*}, \quad \hat{H}_{\mathrm{Z}} = E_{\mathrm{Z}}\sigma_3, \quad \hat{H}_{\mathrm{so}} = \frac{\alpha}{\hbar} p_x \sigma_1, \tag{1b}$$

where m^* is the effective electron mass, E_Z is the Zeeman energy, and α is the SOC strength. The σ_i ($i = 1, 2, 3$) are Pauli matrices operating in spin space, while $E_Z = \frac{1}{2} g\mu_B B_3$ with B_3 a magnetic field applied along the direction of σ_3. We have chosen the most favorable conditions for the development of a topological superconducting phase, where the SOC axis is orthogonal to be magnetic field. Physically, if the SOC is Rashba type the σ_1 axis would be perpendicular to the wire's direction x.

Due to a proximity effect induced by a nearby s-wave bulk superconductor there is a nonzero electron-hole pairing characterized by the energy gap $\Delta_0 = |\Delta|$. Electrostatic gates control the chemical potential μ. The system is described by the

Bogoliubov-deGennes (BdG) equation[40]

$$\mathcal{H}_0 = \int \bar{\Psi}^\dagger(x)\hat{H}_0\bar{\Psi}(x)dx,\ \ \bar{\Psi}^\dagger = \left(\hat{\Psi}^\dagger_\uparrow, \hat{\Psi}^\dagger_\downarrow, \hat{\Psi}_\downarrow, -\hat{\Psi}_\uparrow\right), \quad (2a)$$

$$\hat{H}_0 \left|\phi(t)\right\rangle = \mathrm{i}\hbar\frac{d}{dt}\left|\phi(t)\right\rangle , \quad (2b)$$

$$\hat{H}_0 = \begin{pmatrix} \hat{H}_{0,\mathrm{e}} - \mu & \Delta \\ \Delta^* & \mu - \hat{H}_{0,\mathrm{h}} \end{pmatrix}, \quad (2c)$$

where $\hat{\Psi}_{\uparrow,(\downarrow)}(x)$ is the annihilation operator of electrons with up (down) spin at position x and time t. In Eq. (2c), the quantities μ, Δ and Δ^* are to be interpreted as multiplied by the 2D identity matrix, $\mathbb{1}_{2\times2}$. The Hamiltonian for the holes, $\mu - \hat{H}_{0,\mathrm{h}}$, is obtained by computing the time reversal of $\hat{H}_{0,\mathrm{e}}$,

$$\hat{H}_{0,\mathrm{h}} = \mathcal{T}^{-1}\hat{H}_{0,\mathrm{e}}\mathcal{T} = \sigma_2\hat{H}^*_{0,\mathrm{e}}\sigma_2. \quad (3)$$

where, $\mathcal{T} = -\mathrm{i}\sigma_2 K$, is the time-reversal operator with K the complex conjugation. $\hat{H}_{\mathrm{kin}}$ and $\hat{H}_{\mathrm{so}}$ are TR-symmetry preserving terms in $\hat{H}_{0,\mathrm{e}}$, on the other hand, the sign of the Zeeman contribution, $\hat{H}_{\mathrm{Z}}$, is reversed by the TR operator.

For simplifying treatment on next sections we have written the BdG-Schroedinger equation in Eq.(2a) operating on a ket, $|\phi(t)\rangle$. Indeed, including the case of a BdG time dependent Hamiltonian, $\hat{H}'(t)$, the most natural representation of those states is a Nambu spinor, $\bar{\Phi}(x,t)$ which is written in the basis of $\bar{\Psi}(x,t)$ and evolves satisfying the Schroedinger equation $\left(\hat{H}'(t) - \mathrm{i}\hbar\frac{\partial}{\partial t}\right)\bar{\Phi}(x,t) = 0$. The Nambu field operator allows one to write the fermionic annihilation and creation operator associated with any solution $\bar{\Phi}(x,t)$, this will be useful below; in particular the annihilation operator written in the Schroedinger and Heisenberg picture are

$$\hat{\Phi}_S = \int \bar{\Phi}^\dagger(x,0)\cdot\bar{\Psi}(x)dx = \hat{\Phi}_H(0), \quad (4a)$$

$$\hat{\Phi}_H(t) = \hat{\mathcal{U}}'^\dagger(t,0)\hat{\Phi}_S\hat{\mathcal{U}}'(t,0)\ , \quad (4b)$$

where $\hat{\mathcal{U}}'(t,0)$ is the evolution operator from time 0 to t.

The Hamiltonian $\hat{H}_0$ of Eq. (2a) has been studied extensively. It is known that the system is in the topological superconducting phase for Zeeman energies above a critical value,

$$|E_\mathrm{Z}| > E^\mathrm{c}_\mathrm{Z} \equiv \sqrt{\Delta_0^2 + \mu^2}. \quad (5)$$

This can be seen by solving $\hat{H}_0\bar{\Phi} = E\bar{\Phi}$ for an infinite wire and calculating the Z_2 topological invariant that distinguishes both gapped phases.[11] A topological phase transition involves a closing and reopening of the band gap as a function some parameter,[41] here, the gap closes when $|E_\mathrm{Z}| = E^\mathrm{c}_\mathrm{Z}$. We get insight into the states involved around the critical condition by working at Zeeman energies, $E_\mathrm{Z} = E^\mathrm{c}_\mathrm{Z} + \Delta e_\mathrm{Z}$. We focus on the solutions for small linear momentum $p_x = \hbar k$, the solutions at $|k| \approx k_\mathrm{F}$ are gapped due to the s-wave superconducting pairing. Close to $E = 0$, the solutions organize in two branches which, at the leading order in the wavenumber k, read

$$E^0_\pm(k) = \pm\sqrt{(\alpha k\sin\phi_0)^2 + \Delta e_\mathrm{Z}^2}, \quad (6)$$

with $\phi_0 \equiv \arctan\frac{\Delta_0}{-\mu}$. These solutions are gapless only at the critical Zeeman field, forming a Dirac cone

$$E^0_\pm(k) = \pm\alpha k\sin\phi_0 + O\left(k^2\right) = \pm\alpha k\frac{\Delta_0}{\sqrt{\Delta_0^2+\mu^2}} + O\left(k^2\right). \quad (7)$$

At $k \neq 0$, these branches correspond to states that are the symmetric and antisymmetric combination of states unperturbed by spin-orbit coupling, with energies $E^0_{1,2}(k)\big|_{\alpha=0} = \pm\Delta e_\mathrm{Z} + O\left(k^2\right)$. The unperturbed states are $\bar{\Phi}^0_1 = \left(\cos\frac{\phi_0}{2}, 0, \sin\frac{\phi_0}{2}, 0\right)^\dagger\frac{\mathrm{e}^{\mathrm{i}kx}}{\sqrt{L}}$ and $\bar{\Phi}^0_2 = \left(0, -\sin\frac{\phi_0}{2}, 0, \cos\frac{\phi_0}{2}\right)^\dagger\frac{\mathrm{e}^{\mathrm{i}kx}}{\sqrt{L}}$, where the Nambu-space spin axis is taken along σ_3.

Importantly, for $\Delta e_\mathrm{Z} > 0$ ($\Delta e_\mathrm{Z} < 0$) the solution at $k = 0$ with $E^0 > 0$ is $\bar{\Phi}^0_1$ ($\bar{\Phi}^0_2$). Passing from one situation to the other would imply an abrupt change of such $E^0 > 0$ eigenstate that can only be achieved after a band inversion: at the critical condition the gap closes and both solutions become degenerated. It is not possible then to go from a situation to the other with a smooth deformation of the Hamiltonian without closing and reopening the gap. As mentioned before, this indicates that the two gapped phases are topologically distinct.[41] Notice that the topological trivial phase is identified with the case $E_\mathrm{Z} < \sqrt{\Delta_0^2 + \mu^2}$ because the situation includes the vacuum phase as such is characterized by a chemical potential $\mu < 0$ and very large. Therefore gapless states only appear appear at terminations of the topological phase (with $E_\mathrm{Z} > \sqrt{\Delta_0^2 + \mu^2}$), these terminations may involve interfaces with the trivial phase or with the vacuum.

This kind of midgap states are well-known to appear in Dirac-like equations as a consequence of a sign change in the mass term.[42] For the BdG equation, due to particle-hole symmetry, for each eigenstate with $+E_a$ created with the operator $\hat{\Phi}^\dagger_a$ (taken either in the Heisenberg or the Schroedinger picture, see Eq.(4)) there is another at $-E_a$ which is created with the operator $\hat{\Phi}_a$.[43] Therefore, if a physical system has an eigenstate fulfilling the reality condition, $\hat{\Phi}_a = \hat{\Phi}^\dagger_a$, i.e., being its own antiparticle, it must appear at $E_a = 0$. Furthermore, the zero energy state is protected to local perturbations by the energy gap when it is found unpaired: localized in space and not overlapping spatially with other Majorana solution. Such conditions are fulfilled in the TSP phase in the quantum wire static proposals.

In Sec. III we shall see that the periodically-driven nonmagnetic system we treat here shares a similar topological transition. Such transition is observed both in the Floquet quasienergy spectrum and the associated mean energies. In finite samples Floquet localized states at the edges of the sample appear protected to local disorder and with a well defined quasienergy which is proportional to the driving frequency.

A. SOC-free magnetostatic platform

Consider the joint kinetic and SOC terms in Eqs. (1a) and (1b), $\hat{H}_{\mathrm{kin}} + \hat{H}_{\mathrm{so}} = \frac{1}{2m^*}(p_x + \hbar k_{\mathrm{so}}\sigma_1)^2 - E_{\mathrm{so}}$, with $k_{\mathrm{so}} \equiv \frac{m^*\alpha}{\hbar^2}$ and

$E_{\rm so} \equiv \frac{\hbar^2 k_{\rm so}^2}{2m^*} = \frac{\alpha^2 m^*}{2\hbar^2}$. A spin-dependent shift in momentum,[44] $\hat{U}_1 = \exp(-{\rm i}k_{\rm so}x\sigma_1)$, cancels the SOC term. Since $\hat{U}_1$ rotates the spin an angle $2k_{\rm so}x$ around the σ_1-axis, the Zeeman term— constant in the original Hamiltonian— changes its axis in the (2,3) plane as a function of position. The transformed Hamiltonian, $\hat{H}_{1,\rm e} = \hat{U}_1^\dagger \hat{H}_{0,\rm e}\hat{U}_1$, becomes,[29]

$$\hat{H}_{1,\rm e} = \frac{p_x^2}{2m^*} - E_{\rm so} + E_{\rm Z}\left[\cos(2k_{\rm so}x)\,\sigma_3 + \sin(2k_{\rm so}x)\,\sigma_2\right] . \quad (8)$$

Recently, in Ref. 30, Kjaergaard et al. demonstrated that a system of electrons following Hamiltonian $\hat{H}_{1,\rm e}$ in the presence of a s-wave superconducting pairing potential, Eq.(2), can develop a topological superconducting phase. Starting from arbitrary magnetic textures— generated by, e.g., an engineered array of nearby micromagnets— and by choosing the local magnetic direction as the spin quantization axis, numerical simulations show that the effective SOC arising in the local reference frame can be sufficient for the emergence of topological phases. This results optimal for the sinusoidal magnetic texture of $\hat{H}_{1,\rm e}$, Eq. (8), mapping exactly to the $\hat{H}_{0,\rm e}$ of Eq. (1a), as we already showed by applying the inverse mapping.

Direct comparison with $\hat{H}_{0,\rm e}$ indicates that the amplitude of the rotating magnetic field must be sufficiently *strong* to fulfill the condition of Eq.(5) (the chemical potential in the equation must be replaced by $\mu - E_{\rm so}$ because the energy shift $E_{\rm so}$ is absent in this zero-SOC platform). Therefore, the results of Ref. 30 supports the approach we adopt here for obtaining new physical topological platforms based on removing some interacting terms of interest from a Hamiltonian known to have a topological phase by applying unitary transformations. Remarkably, the approach opens a complete new family of systems able to host topological properties. This is especially interesting in the case of *imperfect* mappings, as for non-sinusoidal magnetic textures in the absence of SOC,[30] where topological properties can still be present.

It is interesting to discuss Eq. (8) from the point of view of spin dynamics of electrons ($\Delta_0 = 0$). Assuming that the wavelength of the magnetic texture ($2\pi k_{\rm so}^{-1}$) is fixed the effective SOC is more significant to the spin dynamics the *weaker* the magnetic field becomes, namely, in the *non-adiabatic* spin evolution regime. Obviously, if the magnetic field amplitude E_Z is fixed the same effect is achieved by decreasing the length $2\pi k_{\rm so}^{-1}$. In these ways, spin eigenstates of Eq. (8) are not fully aligned with the local magnetic field, otherwise no spin mixing survives from the position rotating magnetic field. The *adiabatic* regime is defined in the limit $\omega_{\rm s} \gg 2\pi/t_{\rm c}$, where $\omega_{\rm s} = E_{\rm Z}/\hbar$ is the Larmor frequency of spin precession and $t_{\rm c} = L/v_{\rm F}$ is the time it takes a spin carrier with Fermi velocity $v_{\rm F}$ to cover a characteristic length scale L over which the direction of the magnetic field suffers a significant change (see Ref. 45 and Ref. 46 for a detailed discussion). Non-adiabatic dynamics requires $\omega_{\rm s} \sim 2\pi/t_{\rm c}$.

B. Non-magnetic Floquet platform

Here we get rid of the Zeeman term of Eq. (1a) by applying a global time-dependent rotation to the spins along the magnetic-field axis with an appropriate frequency. For simplicity we first consider the electron block of the Hamiltonian (not the BdG equation) and thus the mentioned transformation is $\hat{U}_{\rm r}(t) \equiv \exp(-{\rm i}\sigma_3 t E_Z/\hbar)$. The time evolution of the rotated states

$$\left|\phi^{\rm rot}(t)\right\rangle \equiv \hat{U}_{\rm r}^\dagger(t)\left|\phi(t)\right\rangle , \quad (9)$$

is given by the equation ${\rm i}\hbar\frac{d}{dt}\left|\phi^{\rm rot}(t)\right\rangle = \hat{H}_{\rm e}(t)\left|\phi^{\rm rot}(t)\right\rangle$, with

$$\begin{aligned} \hat{H}_{\rm e}(t) &\equiv \hat{U}_{\rm r}^\dagger(t)\hat{H}_{0,\rm e}\hat{U}_{\rm r}(t) - {\rm i}\hbar\hat{U}_{\rm r}^\dagger(t)\frac{d\hat{U}_{\rm r}(t)}{dt} \\ &= \hat{U}_{\rm r}^\dagger(t)\hat{H}_{0,\rm e}\hat{U}_{\rm r}(t) - E_{\rm Z}\sigma_3 \\ &= \frac{p_x^2}{2m^*} + \frac{\alpha}{\hbar}p_x\left[\cos\left(2\frac{E_Z}{\hbar}t\right)\sigma_1 - \sin\left(2\frac{E_Z}{\hbar}t\right)\sigma_2\right] . \quad (10) \end{aligned}$$

Where we have used that the equation of motion for the original states, ${\rm i}\hbar\frac{d}{dt}\left|\phi(t)\right\rangle = \hat{H}_{0,\rm e}(t)\left|\phi(t)\right\rangle$. Notice that states $\left|\phi^{\rm rot}(t)\right\rangle$ are, indeed, the interaction-picture states resulting from considering $\hat{H}_{\rm kin} + \hat{H}_{\rm so}$ as a perturbation to $\hat{H}_Z$.[47] This means that a physical system following the time-dependent $\hat{H}_{\rm e}(t)$ *in the Schroedinger picture* can be mapped into the static $\hat{H}_{0,\rm e}$ by the unitary transformation $\hat{U}_{\rm r}(t)$. Since topological phases can arise from $\hat{H}_{0,\rm e}$ when a pairing potential is present, we expect similar features from the periodically driven $\hat{H}_{\rm e}(t)$ in the framework of Floquet theory.

It is clear that the excitations in systems described by either $\hat{H}_{\rm e}(t)$ or $\hat{H}_{0,\rm e}$ are not identical when each of them is assumed to be in the Schroedinger picture. (Even in absence of spin-orbit coupling, where the $\hat{H}_{\rm e}(t)$ results to be *time independent*, actually both Hamiltonians have different energy spectra). However, assuming electron-hole s-wave pairing, both systems share the topological trivial phase. Similarly, for the non-magnetic system with a periodically rotating spin-orbit axis, our mapping allows to predict the existence of a topological phase. As we shall show, the critical magnetic field in the original $\hat{H}_{0,\rm e}$ implies the existence of a *critical driven frequency* in the Floquet system above which a finite piece of wire hosts two Floquet Majorana states localized at its edges. Furthermore, these edge Majorana solutions appear even in the presence of disorder despite the fact that the Majorana Floquet states *are not gapped* in the quasienergy spectrum.

The fact that states responding to the Hamiltonian $\hat{H}_{\rm e}(t)$ can be transformed by a time-dependent unitary mapping to the states responding to $\hat{H}_{0,\rm e}$ is not enough to derive topological properties in $\hat{H}_{\rm e}(t)$. Here, the reason why topological properties are also expected in the time-dependent system lies in the simple nature of $U_{\rm r}(t)$. In general, *any* BdG Hamiltonian $\hat{H}_\Theta(t)$— including those without topological properties— can be mapped into the topological one $\hat{H}_0$ of Eq.(2) (the one based on $\hat{H}_{0,\rm e}$). This is possible provided the unitary transformation is sufficiently complicated to the point of introducing the requirements of the topological phase. More explicitly, starting from the solutions to the arbitrary Hamiltonian,

$(\hat{H}_\Theta(t) - \mathrm{i}\hbar\frac{d}{dt})\left|\phi^\Theta(t)\right\rangle$, the topological Hamiltonian $\hat{H}_0$ governs the time dependence of the transformed states if and only if $\left|\phi^{\rm trans}(t)\right\rangle = \hat{\mathcal{U}}_{\rm top}(t,0)\hat{\mathcal{U}}^\dagger_\Theta(t,0)\left|\phi^\Theta(t)\right\rangle$, where $\hat{\mathcal{U}}_\Theta(t,0)$ and $\hat{\mathcal{U}}_{\rm top}(t,0)$ are the time-evolution operators associated to $\hat{H}_\Theta$ and $\hat{H}_0$, respectively. In our case, $\hat{H}_\Theta = \hat{H}(t)$ [which is the BdG Hamiltonian based on $\hat{H}_{\rm e}(t)$ in presence of a pairing potential, see Eq.(12)], and

$$\hat{U}_{\rm R}(t) \equiv \hat{\mathcal{U}}_{\rm top}(t,0)\hat{\mathcal{U}}^\dagger_\Theta(t,0) = \begin{pmatrix} \hat{U}_{\rm r}(t) & 0 \\ 0 & \hat{U}_{\rm r}(t) \end{pmatrix}$$
$$= \begin{pmatrix} \mathrm{e}^{-\frac{\mathrm{i}}{\hbar}E_Z t} & 0 & 0 & 0 \\ 0 & \mathrm{e}^{\frac{\mathrm{i}}{\hbar}E_Z t} & 0 & 0 \\ 0 & 0 & \mathrm{e}^{-\frac{\mathrm{i}}{\hbar}E_Z t} & 0 \\ 0 & 0 & 0 & \mathrm{e}^{\frac{\mathrm{i}}{\hbar}E_Z t} \end{pmatrix}, \qquad (11)$$

is a rotating-frame spin transformation that does not *introduce* topological superconducting features. Therefore, topological properties in both systems, if any, must be linked. In the following section we show that the solutions of the non-magnetic BdG Hamiltonian based on $\hat{H}_{\rm e}(t)$ in the Schroedinger picture present topological features related to those of $\hat{H}_0$. This is because $\hat{U}_{\rm R}(t)$ establishes a simple mapping between the energy spectrum of the static $\hat{H}_0$ and the Floquet quasienergies of $\hat{H}(t)$. Furthermore, we shall see that each eigenstate of $\hat{H}_0$ is associated with one Floquet quasi-energy state sharing its properties.

III. PROPERTIES OF NON-MAGNETIC PERIODICALLY DRIVEN SYSTEM

We consider a system of electrons described by the time-dependent Hamiltonian of Eq. (10) in the Schroedinger picture. The rotating SOC coexists with a constant s-wave pairing potential, where the corresponding BdG equation reads

$$\mathcal{H}(t) = \int \bar{\Psi}^\dagger(x)\hat{H}(t)\bar{\Psi}(x)dx, \qquad (12a)$$
$$\hat{H}(t) = \begin{pmatrix} \hat{H}_{\rm e}(t) - \mu & \Delta \\ \Delta^* & \mu - \hat{H}_{\rm h}(t) \end{pmatrix}. \qquad (12b)$$

For convenience in the following, we choose the superconducting phase equal to zero, $\Delta = \Delta_0$, we introduce the driving frequency, Ω, a time-dependent SOC vector, $\mathbf{\Lambda}(t)$, and a static SOC vector, $\mathbf{\Lambda}^{(0)}$, rewriting the electron and hole Hamiltonians as

$$\hat{H}_{\rm e}(t) = \hat{H}_{\rm h}(t) = \frac{p_x^2}{2m^*} + \frac{p_x}{\hbar}\left(\mathbf{\Lambda}(t) + \mathbf{\Lambda}^{(0)}\right)\cdot\boldsymbol{\sigma}, \qquad (13)$$

where $\boldsymbol{\sigma} = (\sigma_1, \sigma_2, \sigma_3)$. Equation (13) follows from Eq.(3) after noticing that, for any given time t', $\hat{H}_{\rm e}(t')$ is a time-reversal symmetric operator. For the ideal rotating (IR) case— which is the best candidate for hosting Floquet Majorana fermions— the SOC vectors are,

$$\mathbf{\Lambda}(t) = \mathbf{\Lambda}_{\rm IR}(t) \equiv (\tilde{\alpha}\cos(\Omega t), -\tilde{\alpha}\sin(\Omega t), 0), \qquad (14a)$$
$$\mathbf{\Lambda}^{(0)} = \mathbf{0} \equiv (0,0,0). \qquad (14b)$$

Notwithstanding, we shall also discuss some scenarios away from this ideal situation.

Periodically driven Schroedinger equation and Floquet systems

As discussed in Sec.II B, a 1D system which is subject to a rotating SOC is related to the magnetostatic, topological quantum wire. Time-dependent periodic systems are better described in the context of the Floquet theory. Here we briefly describe such theory. The starting point is the need to solve the Schroedinger equation,

$$\left(\hat{H}(t) - \mathrm{i}\hbar\frac{d}{dt}\right)|\phi(t)\rangle = 0, \qquad (15)$$

for a Hamiltonian periodic in t, $\hat{H}(t) = \hat{H}(t+T)$. Energy is not conserved, however, by virtue of the Floquet theorem the solutions can be written as

$$\left|\phi_a(t)\right\rangle = \mathrm{e}^{-\frac{\mathrm{i}}{\hbar}\varepsilon_a t}\left|\phi_a^T(t)\right\rangle, \qquad (16)$$

where $T = \frac{2\pi}{\Omega}$ is the driving period and $\left|\phi_a^T(t)\right\rangle$ is a periodic state and the subindex a encodes the quantum numbers of the different solutions. We define the Floquet operator $H_{\rm F} \equiv \left(\hat{H}(t) - \mathrm{i}\hbar\frac{d}{dt}\right)$. As $|\phi_a(t)\rangle$ is a solution of the Schroedinger equation then it must hold $H_F\,|\phi_a(t)\rangle = 0$, thus one finds

$$\left(\hat{H}(t) - \mathrm{i}\hbar\frac{d}{dt}\right)\left|\phi_a^T(t)\right\rangle = \varepsilon_a\left|\phi_a^T(t)\right\rangle. \qquad (17)$$

The quasienergies, ε_a, are the eigenvalues of the Floquet operator $H_{\rm F}$. The corresponding eigenvectors are the Floquet quasienergy states (QESs), $\left|\phi_a^T(t)\right\rangle$. Besides, the evolution operator associated to $\hat{H}(t)$ has the form $\hat{\mathcal{U}}(t,t_0) = \boldsymbol{T}_t\exp\left(-\frac{\mathrm{i}}{\hbar}\int_{t_0}^t\hat{H}(t')dt'\right)$, where $\boldsymbol{T}_t$ stands for time-ordering symbol. From Eq.(17) it then follows

$$\hat{\mathcal{U}}(t_0+T, t_0)\left|\phi_a^T(t_0)\right\rangle = \mathrm{e}^{-\frac{\mathrm{i}}{\hbar}\varepsilon_a T}\left|\phi_a^T(t_0)\right\rangle. \qquad (18)$$

Hence, the quasienergies can also be extracted from the phase factors $\mathrm{e}^{-\frac{\mathrm{i}}{\hbar}\varepsilon_a T}$: eigenvalues of the evolution operator over a driving period.

Floquet theorem is equivalent to Bloch theorem for periodic driving instead of position periodic potentials, where quasienergies in Floquet QESs play the role of momenta in Bloch states. The equivalence of solutions belonging to different Brillouin zones in momentum is one of the main signatures of Bloch systems. Similar properties are shared by Floquet systems in the quasienergy axis. This can be seen from Eq. 16, after noticing that states $|\phi_a(t)\rangle$ remains unchanged by the substitution

$$\varepsilon_a \to \varepsilon_a + n\hbar\Omega\,, \quad \left|\phi_a^T(t)\right\rangle \to \mathrm{e}^{\mathrm{i}n\Omega t}\left|\phi_a^T(t)\right\rangle. \qquad (19)$$

Namely, the new Floquet state $\left|\phi_a^{T,n-\rm shift}(t)\right\rangle$ has shifted Fourier components so that for each physical state there are infinite Floquet QESs that are nonorthogonal, with

$\left\langle \phi_a^T(t)|\phi_a^{T,n-\mathrm{shift}}(t)\right\rangle = \mathrm{e}^{\mathrm{i}n\Omega t}$. However, orthogonality is recovered by defining the inner product of Floquet states as the standard inner product averaged over a driving period,

$$\left\langle\left\langle \phi_a^T(t)|\phi_b^T(t)\right\rangle\right\rangle \equiv \frac{1}{T}\int_0^T \left\langle \phi_a^T(t')|\phi_b^T(t')\right\rangle dt' = \delta_{a,b}. \qquad (20)$$

To retain only one QES for each physical state it is sufficient to choose any range of quasienergies of length $\hbar\Omega$— such as $[\varepsilon, \varepsilon{+}\hbar\Omega)$— and discard all the QES outside this region.

The time-dependent Eq. (17) for the Floquet states still needs to be solved. One possibility is to compute the evolution operator and solve Eq. (18). We do this for the case of a finite piece of wire. Alternatively, we can switch to Fourier representation by rewriting the Hamiltonian and the Floquet states as

$$\hat{H}(t) = \sum_{n=-\infty}^{\infty} \mathrm{e}^{-\mathrm{i}\Omega nt}\hat{H}^{(n)}\ , \quad \left|\phi_a^T(t)\right\rangle = \sum_{n=-\infty}^{\infty} \mathrm{e}^{-\mathrm{i}\Omega nt}\left|\phi_a^{(n)}\right\rangle . \qquad (21)$$

By direct substitution in Eq. (17) we find $\sum_m \left(\hat{H}^{(m)} - n\hbar\Omega\delta_{0,m}\right)\left|\phi_a^{(n-m)}\right\rangle = \varepsilon_a\left|\phi_a^{(n)}\right\rangle$, which in matrix representation reads

$$\begin{pmatrix} \ddots & \vdots & \vdots & \vdots & \iddots \\ \cdots & \left(\hat{H}^{(0)} + \hbar\Omega\right) & \hat{H}^{(-1)} & \hat{H}^{(-2)} & \cdots \\ \cdots & \hat{H}^{(1)} & \hat{H}^{(0)} & \hat{H}^{(-1)} & \cdots \\ \cdots & \hat{H}^{(2)} & \hat{H}_{(1)} & \left(\hat{H}^{(0)} - \hbar\Omega\right) & \cdots \\ \iddots & \vdots & \vdots & \vdots & \ddots \end{pmatrix} \begin{pmatrix} \vdots \\ \left|\phi_a^{(-1)}\right\rangle \\ \left|\phi_a^{(0)}\right\rangle \\ \left|\phi_a^{(1)}\right\rangle \\ \vdots \end{pmatrix} = \varepsilon_a \begin{pmatrix} \vdots \\ \left|\phi_a^{(-1)}\right\rangle \\ \left|\phi_a^{(0)}\right\rangle \\ \left|\phi_a^{(1)}\right\rangle \\ \vdots \end{pmatrix} . \qquad (22)$$

This configures a time-independent infinite dimensional eigenvalue problem where ε_a and $\left|\phi_a^{(n)}\right\rangle$ are unknown. Whenever possible, we solve this analytically provided some approximations are introduced, by comparing $\hbar\Omega$ with other energy scales appearing in the Fourier components $\hat{H}^{(n)}$ of Eq. (22). We shall do so only in a small (but important) region in parameter space. For dealing with general situations we resort to a more exact numerical approach.

Mean energy of Floquet quasienergy states

The mean energy of a Floquet QES is defined as the expectation value of the Hamiltonian averaged over one driving period:

$$\begin{aligned} \overline{E}_a &= \frac{1}{T}\int_0^T dt \left\langle \phi_a^T(t)|\hat{H}(t)|\phi_a^T(t)\right\rangle \\ &= \frac{1}{T}\int_0^T dt \left\langle \phi_a^T(t)\left|\hat{H}(t) - \mathrm{i}\hbar\frac{d}{dt} + \mathrm{i}\hbar\frac{d}{dt}\right|\phi_a^T(t)\right\rangle \\ &= \varepsilon_a - \Omega\frac{\partial\varepsilon_a}{\partial\Omega}, \end{aligned} \qquad (23)$$

where we use an extension of the Hellmann-Feynman theorem (for the Floquet operator H_{F}).[48] Notice that computing the set of quasienergies ε_a by fixing Ω— the usual procedure in most numerical treatments of Floquet systems— does not permit the calculation of the associated $\overline{E}_a$. To this aim one needs to either know $\partial\varepsilon_a/\partial\Omega$ or use the periodic time-dependent eigenstate $\left|\phi_a^T(t)\right\rangle$ to compute the integral given in Eq. (23).

Starting from a Floquet state $\left|\phi_a^T(t)\right\rangle$ with quasienergy ε_a, we find that the mean energy is identical for all associated shifted states of Eq. (19) with quasienergy $\varepsilon_a + n\hbar\Omega$, since

$$\overline{E}_a^{n\text{-shift}} = (\varepsilon_a + n\hbar\Omega) - \Omega\frac{\partial}{\partial\Omega}\left(\varepsilon_a + n\hbar\Omega\right) = \overline{E}_a. \qquad (24)$$

In summary, the mean energy is a useful quantity for classifying the Floquet QESs and the physical state $|\phi_a(t)\rangle$ of Eq. (16). Furthermore, very recently, in Ref. 38 Arimondo et al. elaborated on the hypothesis— while comparing with experimental results with apparent success— that the population of Floquet states might follow Bose-Einstein (for bosons) or Fermi-Dirac (for fermions) distributions in the *mean-energy* variable. The latter is an additional motivation towards the study of the mean energies in Floquet systems. An important point we shall address here is how the mean energies of Floquet states behave at both sides of a topological transition.

A. Bulk properties

We now investigate the Floquet solutions of the time-dependent system in its infinitely long version. For arbitrary periodic driving, one must proceed numerically because complexity impedes analytical treatments. For the ideal rotating case our numerical implementation is in full agreement with the analytical results that, as we show in detail below, follows from the mapping to the static topological problem discussed in Sec.II B.

As the system is translational invariant the linear momentum, $p_x = \hbar k$, is a good quantum number; in the following we use the wavenumber k to label the solutions. For a given k, $\hat{H}_k(t)$ is a 4×4 matrix including electron-hole and spin degrees of freedom: the Nambu space. The trial state $|\phi_k(t)\rangle = |k\rangle\,|\varphi_k(t)\rangle$ in the Schroedinger equation (15) leads to a differential equation for the Nambu ket, $|\varphi_k(t)\rangle$:

$$\left(\hat{H}_k(t) - \mathrm{i}\hbar\frac{d}{dt}\right)|\varphi_k(t)\rangle = H_{\mathrm{F}}^{k}\;|\varphi_k(t)\rangle = 0. \tag{25}$$

For each value of k there exist four solutions, we write them as $\left|\varphi_{k,a}(t)\right\rangle$ with $a = 1,\ldots,4$. The knowledge of $\left|\varphi_{k,a}(t)\right\rangle$ allows us to write the solutions as in Eq.(16) by virtue of the Floquet theorem for the periodically driven $\hat{H}_k(t)$.

In order to compute the Floquet solutions we extend the numerical method for the calculation of dispersion relations in spatial lattices given by Ando in Ref. 49. This is performed by discretizing time along a driving period. For each temporal “site” i located at $t_i = i\delta t$ the local Hamiltonian $\hat{H}_k(t_i)$ acts on the Nambu spinor $\varphi_k(t_i)$. The discretized version of the term $-\mathrm{i}\hbar\frac{d}{dt}$ in Eq.(25) provides a hopping term between first-neighbors sites. The discretized H_{F}^{k} can be thought as an effective spatial (in the “sites” t_i) periodic lattice Hamiltonian in Nambu space. The momentum associated to the motion on the lattice t_i is the Floquet quasienergy, ε. Therefore, the Bloch solutions in this effective lattice are the Floquet ones in the time-dependent system, so that by imposing Eq.(25) one obtains ε as the variable that would be the momentum in a spatially periodic lattice. The technical details of the extended Ando method for Floquet systems will be presented elsewhere. The results are equivalent to those found by computing the evolution operator over a period of the driving frequency and then solving the eigenvalue problem of Eq.(18).

1. The IR driving: Floquet bands and Majorana states.

Figure 1 shows numerical results for the time-dependent SOC of Eq.(14), where the SOC axis rotates harmonically around σ_3 axis. As a starting point, in Figs. 1(T.a), 1(C.a) and 1(B.a), we show the dispersion in the absence of driving, corresponding to the eigenenergies $E(k)$ of the static part of the Hamiltonian $\hat{H}^{(0)}$ of Eq. (21). The only interacting term in $\hat{H}^{(0)}$ is the pairing potential, so that electron-hole states are spin-degenerated with eigenenergies

$$E_{\pm,k\sigma} = \pm\sqrt{\Delta_0^2 + \left(\hbar^2k^2/(2m^*) - \mu\right)^2}. \tag{26}$$

These appear as solid lines. Additionally, the same dispersions shifted by an integer multiple of $\hbar\Omega$ are displayed as dashed lines. Those bands are relevant for the time-dependent system since, as shown in Eq.(22), the $\hat{H}^{(m)}$ operators ($m\neq 0$) mix solutions of $\hat{H}^{(0)}$ with energies differing in $m\hbar\Omega$.

The Fourier decomposition of the interacting term $p_x\mathbf{\Lambda}_{\mathrm{IR}}(t)\cdot\sigma/\hbar$ appearing in both $\hat{H}_{\mathrm{e}}(t)$ and $\hat{H}_{\mathrm{h}}(t)$, with $\mathbf{\Lambda}_{\mathrm{IR}}(t)$ given in Eq.(14), determines that the only off-diagonal terms contributing to Eq. (22) are

$$\hat{H}_{\mathrm{e}}^{(\mp 1)} = \hat{H}_{\mathrm{h}}^{(\mp 1)} = \frac{\tilde{\alpha}}{\hbar}p_x\sigma_\pm, \tag{27}$$

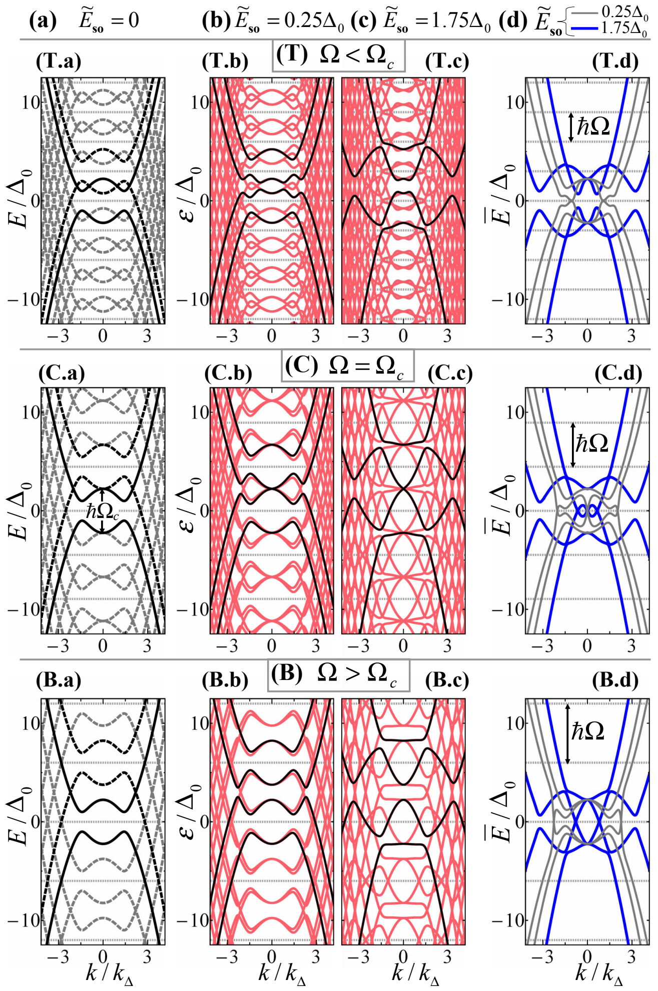

FIG. 1. Ideal rotating (IR) case of Eq.(14): Floquet quasienergies and mean energies. Reference energy and momentum are Δ_0 and $k_\Delta = \sqrt{2m^*\Delta_0}/\hbar$, respectively. We set $\mu = 2\Delta_0$ so that $\hbar\Omega_{\rm c} = 2\sqrt{5}\Delta_0$. Top (T), center (C) and bottom (B) panels show results for $\Omega = 0.9\Omega_{\rm c}$, $\Omega = \Omega_{\rm c}$ and $\Omega = 1.1\Omega_{\rm c}$, respectively. Dotted horizontal lines at $n\hbar\Omega$ are included in all panels. Panels (a) show the spin-degenerated naked dispersion $E_{\pm,k\sigma}$ of Eq. (26) in the absence of the IR SOC-field (solid lines). Dashed lines correspond to $E_{\pm,k\sigma}+m\hbar\Omega$ branches which are important for the mixing due to the periodic driving, see Eq.(22). (b) and (c) Floquet quasienergies ε for finite IR SOC-field of intensity $\tilde{E}_{\rm so} \equiv \tilde{\alpha}^2m^*/(2\hbar^2) = 0.25\Delta_0$ and $1.75\Delta_0$, respectively. Numerical results show an excellent agreement with analytical calculations obtained by mapping the time-dependent problem to the static system having a constant SOC and a finite Zeeman field: the solid black lines depict the four bands of the corresponding static system (shifted in energy by $+\hbar\Omega/2$, see text). Panels (d) show the mean energies $\bar{E}$ of the Floquet states for the simulated IR SOC-field amplitudes. In (C.b) and (C.c), two branches of Floquet solutions close in a Dirac-like quasienergy cone for small k. The reopening of the Dirac cone for $\Omega > \Omega_{\rm c}$, (B.b) and (B.c), indicates a topological phase distinct from that for $\Omega < \Omega_{\rm c}$. The mean energy shows a distinct pattern on each phase (see text and Fig.2).

where $\sigma_\pm = \sigma_1 \pm \mathrm{i}\sigma_2$ are the σ_3-spin raising and lowering operators. This means that the driving introduces mixing between $\hat{H}^{(0)} + m\hbar\Omega$ blocks with $(m - m') = 1$. Due to translation invariance, for each k one needs to solve a time-independent matrix Floquet equation as Eq.(22), where each block is a 4×4 matrix. The amplitude of the IR mixing terms is $\pm\tilde{\alpha}k$. This means that at $k=0$ the system is static and the Floquet treatment is not required. However, in the neighborhood of $k=0$ the system does need Floquet treatment. The energy of the solutions for $k\rightarrow 0$ are $\pm\sqrt{\Delta_0^2+\mu^2}$. For a $\hbar\Omega = 2\sqrt{\Delta_0^2+\mu^2}$, the energies of Floquet blocks with $(m-m')=1$ cross at $k=0$. In particular, the $(m,-)$ band crosses the $(m-1,+)$ one. This situation is illustrated in Fig.1(C.a) as the upper band in solid black line ($m'=0$) crosses the lower band in dashed black line ($m=1$). From this condition we define the critical frequency, $\Omega_{\rm c}$, as,

$$\Omega_{\rm c} \equiv \frac{2}{\hbar}\sqrt{\Delta_0^2+\mu^2}. \tag{28}$$

This $\Omega_{\rm c}$, determined here within Floquet theory, coincides with value predicted by the mapping to the static case introduced in Sec.II B [starting from Eq.(10) by identifying $\Omega=2E_{\rm Z}/\hbar$, Eq.(28) follows from Eq.(5)].

In Figs. 1(C.b) and 1(C.c) we show the resulting Floquet quasienergies at the critical frequency for two different amplitudes of the rotating SOC. For small k we obtain Dirac-cone like quasienergy excitations closing at values

$$\varepsilon_{0,n}(\Omega) \equiv (n+1/2)\hbar\Omega\,, \tag{29}$$

with $\Omega = \Omega_{\rm c}$. They coexist with other bands also closing at $\varepsilon_{0,n}(\Omega_{\rm c})$, but with vanishing $\partial\varepsilon/\partial k$. The bands do not longer close at $k\approx 0$ for either $\Omega < \Omega_{\rm c}$ [shown in Fig.1(T.b) and Fig.1(T.c)] or $\Omega > \Omega_{\rm c}$ [shown in Figs. 1(B.b) and 1(B.c)]. Such opening and closing of quasienergy bands suggest a change in topology. However, here the full quasienergy spectrum is gapless as the solutions for larger k take all possible quasienergy values.

At this point it is clarifying to make use of the mapping introduced in Sec.II B, where the Floquet solutions can be obtained from the static solutions of the SOC plus Zeeman 1D superconducting system. We start from the eigenstates of $\hat{H}_0$ with energy E_a [see Eqs. (1b) and (2a)]

$$\left|\phi_a^0(t)\right\rangle \rightarrow \mathrm{e}^{-\frac{\mathrm{i}}{\hbar}E_a t}\bar{\Phi}_a^0(x), \tag{30}$$

with $\bar{\Phi}_a^0(x)$ a Nambu spinor satisfying $(\hat{H}_0 - E_a)\bar{\Phi}_a^0(x) = 0$. The $\hat{H}_0$ eigenenergies for the infinite case are distributed in four bands,[6]

$$E_a = E_{b_1,b_2}(k) = b_1\left[\Delta_0^2+E_{\rm Z}^2+\left(\frac{\hbar^2k^2}{2m^*}-\mu\right)^2+\alpha^2k^2 +b_2\sqrt{\Delta_0^2E_{\rm Z}^2+\left(\frac{\hbar^2k^2}{2m^*}-\mu\right)^2\left(\alpha^2k^2+E_{\rm Z}^2\right)}\right]^{1/2}, \tag{31}$$

with $b_1=\pm$ and $b_2=\pm$. The spin rotation of Eq.(11) applied on the static solutions give

$$|\phi_a(t)\rangle \equiv \hat{U}_{\rm R}^\dagger(t)\left|\phi_a^0(t)\right\rangle \;\rightarrow\; \bar{\Phi}_a(x,t), \tag{32}$$

which are the solutions of the non-magnetic IR SOC superconducting 1D system by substituting $E_Z \rightarrow \hbar\Omega/2$ and $\alpha\rightarrow\tilde{\alpha}$.

The physical state $|\phi_a(t)\rangle$, Eq.(16), can be associated to a family of Floquet QESs, the members of such family have quasienergies differing in multiples of $\hbar\Omega$. Disregarding such an ambiguity, Eq.(32) is important to determine the quasienergy values associated to the solution with energy E_a of the static quantum-wire. For convenience, we first write each eigenstate of the static system of Ref. 6 (assumed known) as a Nambu spinor, $\bar{\Phi}_a^0(x) = (A_a(x),B_a(x),C_a(x),D_a(x))^T$. We cast the resulting physical state in the form $|\phi_a(t)\rangle = \mathrm{e}^{-\frac{\mathrm{i}}{\hbar}\varepsilon_a t}\left|\phi_a^T(t)\right\rangle$, this allow us to identify of the quasienergy for the time-dependent system as

$$\varepsilon_a = E_a + (n+1/2)\hbar\Omega = E_a + \varepsilon_{0,n}(\Omega), \tag{33}$$

and the associated Floquet QES as the Nambu spinor

$$\bar{\Phi}_a^T(x,t) = \mathrm{e}^{\mathrm{i}n\Omega t}\begin{pmatrix} A_a(x)\mathrm{e}^{\mathrm{i}\Omega t} \\ B_a(x) \\ C_a(x)\mathrm{e}^{\mathrm{i}\Omega t} \\ D_a(x)\end{pmatrix}. \tag{34}$$

Importantly, Eqs.(34) and (33) are valid also for cases in which both linked systems are not translational invariant and thus the solutions are not eigenstates of the momentum p_x; for example in Sec.III B we deal with finite and disordered systems.

We set $n=0$ in Eq.(33) to generate Floquet quasienergies of the IR case using the energies of the static system given in Eq.(31). We plot in black solid lines the resulting ε_a in panels (b) and (c) of Fig.1, i.e., for different driving frequencies and Rashba strengths. Floquet quasienergies obtained entirely within the Floquet picture with our numerical method show an excellent agreement with the analytical results. In Figs. 1(C.b) and 1(C.c) for $\Omega = \Omega_{\rm c}$ we see that the Floquet-Dirac branches closing at $\varepsilon_{0,n}(\Omega_{\rm c})$ map to the Dirac-cone branches of $\hat{H}_0$ that close at $E_a=0$ (those with nonvanishing $\partial\varepsilon/\partial k$ at $k=0$). In the plot, we have chosen $\mu > \Delta_0$ to show that the mapping holds in general. It is known that the $\mu=0$ case is the most favorable for expressing the Kitaev model in the static $\hat{H}_0$ because the effective p-wave gap is larger.[17] Here, $\mu > \Delta_0$ assures a nonzero electron density allowing the development of superconductivity by proximity effect when switching off de driving ($\tilde{\alpha}=0$).

In the static system, as discussed above, the closing and reopening of the band gap indicates a change in topological properties. There, when MFs are present, they appear as solutions of the BdG equation with $E_a = E_{\rm MF} = 0$. This follows from the particle-hole symmetry of the BdG Hamiltonian that enforces zero energy for any eigenstate which is its own antiparticle. In the translational invariant system $E_a = 0$ solutions only appear at the critical Zeeman energy for $k=0$. Either in extended or finite systems, the general form of a Majorana fermion in Nambu space is[43] $\bar{\Phi}_{\rm MF}^0(x,t) = \left(A_{\rm MF}(x), B_{\rm MF}(x), B_{\rm MF}^*(x), -A_{\rm MF}^*(x)\right)^T$, and thus the associated fermionic operator is (because $E_a=0$ both the Schroedinger and the Heisenberg picture lead to the same operator, see Eq.(4))

$$\hat{\Phi}^0_{\mathrm{MF}} = \hat{\Phi}^{0\,\dagger}_{\mathrm{MF}} = \int dx\Big[A_{\mathrm{MF}}(x)\hat{\Psi}_\uparrow(x) + A^*_{\mathrm{MF}}(x)\hat{\Psi}^\dagger_\uparrow(x) + B_{\mathrm{MF}}(x)\hat{\Psi}_\downarrow(x) + B^*_{\mathrm{MF}}(x)\hat{\Psi}^\dagger_\downarrow(x)\Big]. \qquad (35)$$

A natural question arising here is whether the existence of Majorana solutions in the static system dictates the existence of Majorana solutions in the IR system of Eq.(12a). To see this, we construct the solution of the driven IR system which is associated to the static MF solution of $\hat{H}_0$; in the Nambu spinor representation this is just $\bar{\mathit{\Phi}}_{\mathrm{FMF}}(x,t) = \hat{U}^\dagger_{\mathrm{R}}(t)\bar{\mathit{\Phi}}^0_{\mathrm{MF}}(x,t)$, we get

$$\bar{\mathit{\Phi}}_{\mathrm{FMF}}(x,t) = \begin{pmatrix} A_{\mathrm{MF}}(x)\mathrm{e}^{\frac{\mathrm{i}}{2}\Omega t} \\ B_{\mathrm{MF}}(x)\mathrm{e}^{-\frac{\mathrm{i}}{2}\Omega t} \\ B^*_{\mathrm{MF}}(x)\mathrm{e}^{\frac{\mathrm{i}}{2}\Omega t} \\ -A^*_{\mathrm{MF}}(x)\mathrm{e}^{-\frac{\mathrm{i}}{2}\Omega t} \end{pmatrix}. \qquad (36)$$

we see that this state satisfies the particle-antiparticle condition while it evolves periodically in time [this follows from Eq.(4) noting that $\hat{\Phi}_H(t) = \hat{\mathcal{U}}'^{\dagger}(t,0)\hat{\Phi}_H(0)\hat{\mathcal{U}}'(t,0)) = \hat{\Phi}_H(t)^\dagger$]: it is a Floquet Majorana fermion (FMF). Notice that two driving periods are needed for the time-dependent state to revisit the same instantaneous configuration. This is so because the $\hat{U}_{\mathrm{R}}(t)$ of Eq. (11) is made of spin-1/2 operators with rotation angle $2\pi t/T$ (see Sec.III A 2). For $t = 2nT$ (rotation angle $4\pi n$), it reduces to the identity. This is consistent with the fact that a representation within Floquet theory of such a MF state— $E_a = 0$ in Eq.(33)— must have quasienergy

$$\varepsilon_{\mathrm{FMF}} = \varepsilon_{0,n}(\Omega) = (n + 1/2)\hbar\Omega, \qquad (37)$$

meaning that FMF states acquire a phase of $\pi + 2\pi n$ (i.e., a factor -1) after one driving period. At $\Omega = \Omega_{\mathrm{c}}$, the latter coincide with the quasienergies at which the Floquet-band gaps (those with $k \approx 0$) close.

Similar FMFs with finite quasienergy were reported by Jiang et al. in Ref. 9, where they studied a BEC cold-atom quantum wire subject to static SOC and magnetic field with a periodically modulated chemical potential. Their results demonstrates that finite-quasienergy FMFs are not restricted to our particular model. An important point that Jiang et al. brought upon is that the BdG-Floquet operator preserves electron-hole symmetry. In his context this means that for each Floquet state with quasienergy $+\varepsilon_a$ created with the operator $\hat{\Phi}^\dagger_a$ (see Eq.(4)) there is another at $-\varepsilon_a$ which is created with the operator $\hat{\Phi}_a$. Because quasienergies differing in $n\hbar\Omega$ lead to equivalent physical solutions this means that the Majorana condition ($\hat{\Phi}^\dagger_a = \hat{\Phi}_a$) can also be satisfied by states at exactly the nonzero quasienergies given in Eq.(37). We shall return to the discussion of unpaired FMFs in Sec.III B as bounded states appearing at the edges of topological systems are intrinsic to the finite size samples treated there.

2. *The IR driving: topological properties*

We have successfully established a link between the eigenenergies E_a (eigenstates $\big|\phi^0_a(t)\big\rangle$) of the static quantum wire of Ref. 6, $\hat{H}_0$, and the quasienergies ε_a (Floquet states $\big|\phi^T_a(t)\big\rangle$) of our proposed non-magnetic system, $\hat{H}(t)$. We have shown, using the exact mapping, that for each Majorana solution appearing in the static system there is an analog Floquet Majorana fermion appearing in the driven system. Those FMFs are protected by the *same energy gap* that the associated MFs in the static system.

In order to make even more explicit that the topological properties of the Floquet system are equivalent to those in the static system we make use of our mapping to write the evolution operator for the rotating states. From Eq.(32) at $t = 0$ the initial state in both pictures is the same,

$$\big|\phi_a(0)\big\rangle = \big|\phi^0_a(0)\big\rangle. \qquad (38)$$

Because of the time-independence of $\hat{H}_0$ we can write the time evolved state in the static system as,

$$\big|\phi^0_a(t)\big\rangle = \exp\left(-\frac{\mathrm{i}}{\hbar}\hat{H}_0 t\right)\big|\phi^0_a(0)\big\rangle. \qquad (39)$$

In order to simulate the time-dependent system with the IR excitation, the amplitudes of the interactions in Eq.(1b) are chosen as $\alpha \to \tilde{\alpha}$ and $E_Z \to \hbar\Omega/2$. Introducing Eq.(38) and Eq.(39) in Eq.(32) we write the evolution in the time-dependent system as,

$$|\phi_a(t)\rangle = \hat{\mathcal{U}}(t,0)\,|\phi_a(0)\rangle, \qquad (40a)$$

$$\hat{\mathcal{U}}(t,0) \equiv \hat{U}^\dagger_{\mathrm{R}}(t)\exp\left(-\frac{\mathrm{i}}{\hbar}\hat{H}_0 t\right). \qquad (40b)$$

After replacing $E_Z \to \hbar\Omega/2$ in Eq.(11) we get $\hat{U}^\dagger_{\mathrm{R}}(T) = -\mathbb{1}_4$, this is a 2π angle spin rotation, with $\mathbb{1}_4$ the identity in the Nambu space (in the same basis as $\hat{H}_0$ given in Eq.(2c)). Therefore, when particularizing $\hat{\mathcal{U}}(t,0)$ for the evolution over a full period we get

$$\hat{\mathcal{U}}(T,0) = \exp\left(-\frac{\mathrm{i}}{\hbar}\hat{H}_{\mathrm{eff}}T\right), \qquad (41a)$$

$$\hat{H}_{\mathrm{eff}} \equiv \hat{H}_0 + \mathbb{1}_4\varepsilon_{0,n}(\Omega), \qquad (41b)$$

This means that the evolution over a period in the time-dependent system, $\hat{\mathcal{U}}\,(T,0) = \mathbf{T}_t \exp\,(-\frac{\mathrm{i}}{\hbar}\int_0^T \hat{H}(t')dt')$, is equivalent to the evolution over the same period T with the time-independent effective Hamiltonian, $\hat{H}_{\mathrm{eff}}$. Not surprisingly, the effective Hamiltonian is just $\hat{H}_0$ trivially shifted in energy by the amount $\varepsilon_{0,n}(\Omega) = (n + 1/2)\hbar\Omega$ defined in Eq.(29). In the light of Eq.(18), such shift justifies the form of the quasienergies in Eq.(33).

As pointed out by Kitagawa et al. in Ref. 18, the topological properties contained in the effective Hamiltonian of a Floquet system are to be studied with the tools for time-independent topological phase transitions. The topological phases appearing in $\hat{H}_{\mathrm{eff}}$ imply associated topological phases in the Floquet system. We can now formally conclude that the same topological invariant, a Z_2 number,[11] which is different in the two gapped phases of the static and magnetic model of Ref. 6 is also identifying the two Floquet topological phases in the nonmagnetic driven system. In particular this corroborates that the regime with $\Omega > \Omega_{\rm c}$ (supercritical) is indeed a Floquet topological superconducting phase whereas for $\Omega < \Omega_{\rm c}$ (subcritical) is to be associated with the topological trivial superconducting phase.

3. The IR driving: mean energies

We now discuss the mean energies of the Floquet states depicted in Figs. 1(T.d), 1(C.d) and 1(B.d). These follow from Eq.(23) after calculating the derivatives $\partial\varepsilon_a/\partial\Omega$. The numerical results agree with the analytical mean energies derived from Eq.(31) by computing

$$\overline{E}_a = E_a - E_Z \frac{\partial E_a}{\partial E_Z}\,, \tag{42}$$

and substituting $E_Z \to \hbar\Omega/2$. At critical frequency, $\Omega = \Omega_{\rm c}$, the two Floquet states with quasienergy forming a Dirac cone— see black solid lines in Figs. 1(C.b) and 1(C.c)— lead to linear mean-energy dispersions around $k = 0$ as shown in Fig. 1(C.d). We verified that this happens as a general rule, where the mean-energy bands closing the gap at $\overline{E} = 0$ derive from the Floquet-quasienergy bands closing at $\varepsilon_{0,n}(\Omega_{\rm c})$.

As a result of a discontinuity in the mean-energy bands as a function of the driving frequency, these get very sensitive at $\Omega_{\rm c}$ for small k. Such a discontinuity is intimately related to the change of topological properties. Right at $k=0$, the amplitude of periodic driving vanishes and the mean energy simply reduces to the energy, $\overline{E}_\pm(k=0) = \pm\sqrt{\Delta_0^2+\mu^2} = \hbar\Omega_{\rm c}/2$. Below the critical frequency, the top mean-energy band is connected to the $\overline{E}_+(k=0)$ point while the bottom band acts likewise with the $\overline{E}_-(k=0)$ point, instead. Remarkably, above the critical frequency this relationship is inverted. The inversion point is defined at $\Omega_{\rm c}$, where linear dispersion in mean energy is developed excluding the states with $k = 0$: points $\overline{E}_\pm(k=0)$ appear isolated from the bands (see following discussion and Fig. 2 for details). In general, for higher k the mean-energy spectrum is complicated, this is particular for the case shown $\mu > \Delta_0$. For $\mu \approx 0$ the mean-energy bands very much resemble those of the energy of the static system for $\Omega = \Omega_{\rm c}$, away from the critical condition the low k mean energies are always different than the energies of the static system.[50]

For a better understanding of criticality in the vicinity of $\Omega_{\rm c}$, it is useful to solve the Eq.(22) for the Floquet operator in the limits of $\mu \ll \Delta_0$ and small k. We first need the solutions of the static component of $\hat{H}(t)$, i.e., $\hat{H}^{(0)}$, in the Nambu basis with spin quantized along the 3-axis, $(\psi_\uparrow^\dagger, \psi_\downarrow^\dagger, \psi_\downarrow, -\psi_\uparrow)^\dagger$. For simplicity, we define Nambu unit vectors as $\widehat{\psi}_l \equiv (\delta_{1,l}, \delta_{2,l}, \delta_{3,l}, \delta_{4,l})^T$. As $\hat{H}^{(0)}$ only includes the kinetic term and the pairing potential, we define the angle $\varphi_k \equiv \arctan\left(\Delta_0/(\hbar^2k^2/(2m^*) - \mu)\right)$. The solutions are

$$|+, k\uparrow\rangle = \frac{\mathrm{e}^{\mathrm{i}kx}}{\sqrt{L}}\left(\cos\frac{\varphi_k}{2}\widehat{\psi}_1 + \sin\frac{\varphi_k}{2}\widehat{\psi}_3\right) \tag{43a}$$

$$|+, k\downarrow\rangle = \frac{\mathrm{e}^{\mathrm{i}kx}}{\sqrt{L}}\left(\cos\frac{\varphi_k}{2}\widehat{\psi}_2 + \sin\frac{\varphi_k}{2}\widehat{\psi}_4\right) \tag{43b}$$

$$|-, k\uparrow\rangle = \frac{\mathrm{e}^{\mathrm{i}kx}}{\sqrt{L}}\left(\sin\frac{\varphi_k}{2}\widehat{\psi}_1 - \cos\frac{\varphi_k}{2}\widehat{\psi}_3\right) \tag{43c}$$

$$|-, k\downarrow\rangle = \frac{\mathrm{e}^{\mathrm{i}kx}}{\sqrt{L}}\left(\sin\frac{\varphi_k}{2}\widehat{\psi}_2 - \cos\frac{\varphi_k}{2}\widehat{\psi}_4\right) \tag{43d}$$

with the energies given in Eq.(26). These states are, indeed, eigenstates of each block $\hat{H}^{(0)} + m\hbar\Omega$ of the Floquet operator given in Eq.(22). We define $|m, \pm, k\sigma\rangle \equiv \mathrm{e}^{\mathrm{i}m\Omega t}\,|\pm, k\sigma\rangle$ for referring to the eigenstates of block m by simply introducing a Fourier phase factor.

We limit our analysis only to blocks $m = 0$ and $m = 1$ in Eq.(22), assuming the mixing of few bands only. This is justified since: (i) the only mixing components in $\hat{H}(t)$ due to the periodic driving are $\hat{H}^{(\pm1)}$, (ii) in the small k limit the time dependent components are small, discouraging mixing of states far apart in energy, (iii) close to the critical frequency, $\Omega = \Omega_{\rm c} + \delta\epsilon/\hbar$, other states with small k are at least $\hbar\Omega_{\rm c}$ away in quasienergy, and (iv) other choices with $m - m' = 1$ lead to shifted quasienergies (in multiples of $\hbar\Omega$) and, therefore, to equivalent solutions. Furthermore, we restrict the Floquet operator to the subspace of $|0, +, k\sigma\rangle$ and $|1, -, k\sigma\rangle$, i.e., the four states crossing when $\Omega = \Omega_{\rm c}$.

Combining Eqs. (27) and (12) up to linear order in k, the Floquet operator of Eq.(22) reduces to

$$\widetilde{H}_{\rm F} = \begin{pmatrix} \hbar\Omega_{\rm c}/2 & 0 & 0 & 0 \\ 0 & \hbar\Omega_{\rm c}/2 & \tilde{\alpha}k\sin\varphi_0 & 0 \\ 0 & \tilde{\alpha}k\sin\varphi_0 & \hbar\Omega_{\rm c}/2 + \delta\epsilon & 0 \\ 0 & 0 & 0 & \hbar\Omega_{\rm c}/2 + \delta\epsilon \end{pmatrix}, \tag{44}$$

in the ordered basis $\{|0, +, k\uparrow\rangle, |0, +, k\downarrow\rangle, |1, -, k\uparrow\rangle, |1, -, k\downarrow\rangle\}$. We readily notice that the 1st and 4th states

$$\left|\phi_1^T(t)\right\rangle = |+, k\uparrow\rangle \qquad \text{with } \varepsilon_1 = \hbar\Omega_{\rm c}/2, \tag{45a}$$

$$\left|\phi_2^T(t)\right\rangle = |-, k\downarrow\rangle\,\mathrm{e}^{\mathrm{i}\Omega t} \quad \text{with } \varepsilon_2 = \hbar\Omega_{\rm c}/2 + \delta\epsilon, \tag{45b}$$

do not mix under the action of the rotating SOC axis. Their mean energy, Eq.(23), is identical to their energy:

$$\overline{E}_1 = \hbar\Omega_{\rm c}/2\,,\ \ \overline{E}_2 = -\hbar\Omega_{\rm c}/2, \tag{46}$$

where we used that $\partial\Omega_{\rm c}/\partial\Omega = 0$ and $\partial(\delta\epsilon)/\partial\Omega = \hbar$. The remaining two solutions, for $k \neq 0$, are a mixture of states with different m. By defining the angle $\eta_k \equiv \arctan\left(2\tilde{\alpha}k\sin\varphi_0/\delta\epsilon\right)$, these solutions

$$\left|\phi_3^T(t)\right\rangle = \cos\frac{\eta_k}{2}\,|+, k\downarrow\rangle - \sin\frac{\eta_k}{2}\,|-, k\uparrow\rangle\,\mathrm{e}^{\mathrm{i}\Omega t}, \tag{47a}$$

$$\left|\phi_4^T(t)\right\rangle = \sin\frac{\eta_k}{2}\,|+, k\downarrow\rangle + \cos\frac{\eta_k}{2}\,|-, k\uparrow\rangle\,\mathrm{e}^{\mathrm{i}\Omega t}, \tag{47b}$$

with quasienergies,

$$\varepsilon_3(k) = \hbar\Omega_c/2 + \frac{1}{2}\delta\epsilon - \sqrt{\left(\frac{\delta\epsilon}{2}\right)^2 + (\tilde{\alpha}k\sin\varphi_0)^2}, \quad (48a)$$

$$\varepsilon_4(k) = \hbar\Omega_c/2 + \frac{1}{2}\delta\epsilon + \sqrt{\left(\frac{\delta\epsilon}{2}\right)^2 + (\tilde{\alpha}k\sin\varphi_0)^2}. \quad (48b)$$

At the critical frequency, $\delta\epsilon = 0$, the two branches form a Dirac cone in quasienergy. The vertex at $k = 0$ lies at quasienergy $\hbar\Omega_c/2$ (while the l-shifted solutions cross at $\hbar\Omega_c/2 + l\hbar\Omega_c = \varepsilon_{l,0}(\Omega_c)$). The superconducting gap is essential since the mixing term $\tilde{\alpha}k\sin\varphi_0$, with $\sin\varphi_0 = -\Delta_0/\sqrt{\Delta_0^2 + \mu^2}$, vanishes for $\Delta_0 = 0$ (leading to flat dispersions).

For arbitrary values of k (always in the small k approximation) the mean energies for these two solutions are

$$\overline{E}_3(k) = -\overline{E}_4(k) = \frac{\delta\epsilon\hbar\Omega_c/2 - 2(\tilde{\alpha}k\sin\varphi_0)^2}{\sqrt{\delta\epsilon^2 + 4(\tilde{\alpha}k\sin\varphi_0)^2}}. \quad (49)$$

At the critical frequency, $\delta\epsilon = 0$, the two branches form a Dirac cone in mean energy, $\pm|\tilde{\alpha}k\sin\varphi_0|$. This excludes the case $k = 0$, with mean energies fixed at $\pm\hbar\Omega_c/2$. We find

$$\overline{E}_3(0) = -\overline{E}_4(0) = \begin{cases} -\frac{\hbar}{2}\Omega_c, & \text{for } \Omega < \Omega_c \\ \frac{\hbar}{2}\Omega_c, & \text{for } \Omega > \Omega_c. \end{cases} \quad (50)$$

In Fig.2 we show the different behavior of the quasienergies and mean energies involved around the transition, i.e., the solutions 3 and 4 in the latter derivation. For simplicity only the bottom quasienergy [mean-energy] band is plotted in the plane (Ω, k) in Fig.2(a) [Fig.2(g)]. The low-k quasienergy band passes through the transition without visible change (see upper panels in Fig.2(b) to Fig.2(f)); on the other hand the mean-energy band (lower panels in Fig.2(b) to Fig.2(f)) clearly allows to distinguish the two sides of the transition. Both the abrupt change in mean energy and the Dirac-cone dispersion at the critical parameter are due to the band inversion and linear-in-k mixing underlying the phase transition. The result here is consistent with what is commonly found in Floquet systems, i.e., avoided crossings in quasienergy producing abrupt changes in the associated mean energies.[51]

In our study of the Floquet problem, the need to compute the mean energies $\overline{E}_a$ arises naturally. The emergence of the mean energy as an indicator of the band inversion is remarkable. It is therefore pertinent to ask whether $\overline{E}_a$ is a meaningful quantity to be computed in static systems those discussed in Ref. 6 or even in more general contexts. We have shown that $\overline{E}_a$ can be derives from Eq.(42) as a function of the eigenvalues of the static system. By choosing an eigenstate of $\hat{H}_0$, $\left|\phi_a^0(t)\right\rangle$, and applying the Hellmann-Feynman theorem we find that $\overline{E}_a$ is just the expectation value in state $\left|\phi_a^0(t)\right\rangle$ of the Hamiltonian operator *without* the part proportional to E_Z, i.e. without the Zeeman interaction. In other words $\overline{E}_a$ is the expectation value in $\left|\phi_a^0(t)\right\rangle$ (eigenstate of the full Hamiltonian)

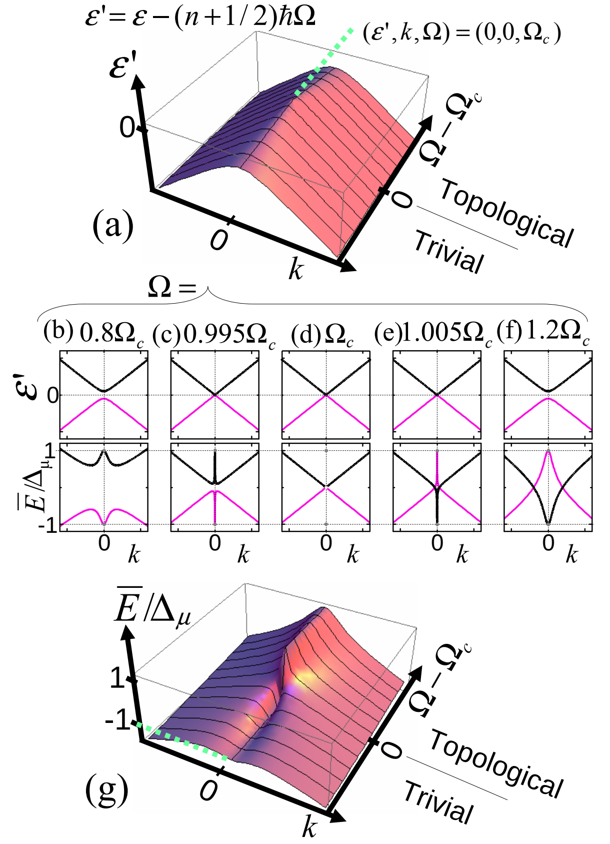

FIG. 2. (a) Quasienergies $\varepsilon' = \varepsilon - \varepsilon_{0,n}(\Omega)$ and (g) mean energies $\overline{E}$ of Floquet states as a function on the driving frequency Ω and the linear momentum $\hbar k$. In the plot $\Delta_\mu \equiv \hbar\Omega_c/2 = \sqrt{\Delta_0^2 + \mu^2}$. We focus on the solutions that are affected by the ideal rotating SOC driving in the small k limit for $\mu \ll \Delta_0$, given in Eq.(47). For the sake of clarity, surface plots show the lower energy bands only (see $\varepsilon_3(k)$ and $\overline{E}_3(k)$ in the text): upper bands follow by symmetry ($\varepsilon_4(k) = -\varepsilon_3(k)$ and $\overline{E}_4(k) = -\overline{E}_3(k)$). In panels (b), (c), (d), (e) and (f), the driving frequency Ω is fixed and both bands are shown. At the critical frequency— panel (d)— the quasienergies form a Dirac-cone while the mean energies show a similar behavior except for a discontinuity at $k = 0$. Just away from Ω_c, sub- and super-critical regimes can not be distinguished from the quasienergy bands alone. In contrast, thanks to the discontinuity developed at the critical point, the mean-energy bands show remarkable features distinguishing one regime from another. Such a contrast is clearly seen already in the surface plots of panels (a) and (g).

of the operator obtained by enforcing $E_Z = 0$ in $\hat{H}_0$. Similarly, two other indicators of the band inversion can be constructed here: the expectation value of $\hat{H}_0$ evaluated at $\Delta_0 = 0$,

$$E_a - \Delta_0\frac{\partial E_a}{\partial \Delta_0}, \quad (51)$$

and the expectation value of $\hat{H}_0$ evaluated at $\mu = 0$,

$$E_a - \mu\frac{\partial E_a}{\partial \mu}. \quad (52)$$

Such expectation-value indicators, I_ζ (here $\zeta = \{E_Z, \mu, \Delta_0\}$), can be constructed from the eigenvalues E_a with great generality to deal with band inversions. Physically, this is not surprising since the complements of I_ζ, namely, $E_a - I_\zeta$ are the expectation values in the eigenstate of operators appearing in the Hamiltonian. As discussed in Sec.II here the $k \approx 0$ eigenstates of the bands involved in the topological phase transition change abruptly when passing through the critical condition, this justifies the observed behavior. Here, we do not discuss these indicators further as they are beyond the scope of this work.

4. *Other forms of SOC driving beyond IR case*

We have shown that the topological system of Ref. 6 is directly related to Floquet system composed of a non-magnetic superconducting wire subject to a rotating SOC axis. The studied time-dependent Hamiltonian satisfies: (i) Fourier decomposition has only zero frequency and $\pm\Omega$ components, (ii) the zero frequency component of the Hamiltonian has no SOC contribution, (iii) the ideal SOC rotation introduces a spin symmetry around the 3-axis, and (iv) the choice of one out of two possible rotational senses for the SOC axis determines the breaking of time-reversal symmetry (needed for emergence of Majorana fermions at the boundary of the topological region).[43] Here, we briefly discuss the Floquet quasienergies and mean energies in systems satisfying only some of the above conditions. Notice, however, that a more rigorous study of the situations below would require analyzing each of their effective Hamiltonians (see Eq.(41)).

In Fig. 3 we present a sketch of the ideal rotating SOC, panel (a), together with two alternative types of SOC drivings, panels (b) and (c). Figure 3(b) depicts a linear (L) driving $\boldsymbol{\Lambda}_{\mathrm{L}}(t)$, such that

$$\begin{aligned} &\boldsymbol{\Lambda}_{\mathrm{L}}(t)\cdot\boldsymbol{\sigma} \equiv \boldsymbol{\Lambda}_{\mathrm{IR}}(t)\cdot\boldsymbol{\sigma} + \sigma_1(\boldsymbol{\Lambda}_{\mathrm{IR}}(t)\cdot\boldsymbol{\sigma})\sigma_1, \\ \Rightarrow\quad &\boldsymbol{\Lambda}_{\mathrm{L}}(t) = (2\tilde{\alpha}\cos(\Omega t), 0, 0)\,. \end{aligned} \tag{53}$$

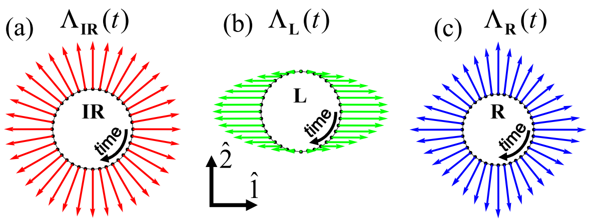
(a)
$\Lambda_{\mathbf{IR}}(t)$
IR
time
(b)
$\Lambda_{\mathbf{L}}(t)$
L
time
$\hat{2}$
$\hat{1}$
(c)
$\Lambda_{\mathbf{R}}(t)$
R
time

FIG. 3. Sketch of three different cases for the periodic SOC driving $\boldsymbol{\Lambda}(t)$ of Eq. (13). (a) Ideally rotating (IR) driving $\boldsymbol{\Lambda}_{\mathrm{IR}}(t)$ of Eq. (14): the SOC axis rotates uniformly in the $1-2$ plane with constant coupling strength. (b) Linear (L) driving $\boldsymbol{\Lambda}_{\mathrm{L}}(t)$ of Eq. (53): the orientation of the SOC is fixed while the coupling strength oscillates harmonically. (c) Ramp (R) rotation driving $\boldsymbol{\Lambda}_{\mathrm{R}}(t)$ of Eq. (55): the SOC axis rotates anharmonically in the $1-2$ plane with varying coupling strength driven by symmetrical triangular waves

.

This represents the superposition of clockwise and counterclockwise IR rotations with the same amplitude $\tilde{\alpha}$. This driving does not fulfill property (iii) of the IR case since the SOC strength oscillates while the axis direction is preserved. The Fourier amplitudes are

$$\hat{H}^{(\pm1)}_{\mathrm{e,L}} = \hat{H}^{(\pm1)}_{\mathrm{h,L}} = 2\frac{\tilde{\alpha}}{\hbar}p_x\sigma_1 = 2\frac{\tilde{\alpha}}{\hbar}p_x(\sigma_+ + \sigma_-)\,. \tag{54}$$

This means that the reduced Floquet operator for the L driving mixes not only states $|0,+,k\downarrow\rangle$ and $|1,-,k\uparrow\rangle$, as in the IR case of Eq.(44), but also states $|0,+,k\uparrow\rangle$ and $|1,-,k\downarrow\rangle$. This extra mixing is a consequence of the violation of property (iv), leading to the double-degeneracy of the full quasienergy spectrum, as we shall see below.

Figure 3(c) depicts a different kind of rotation defined by

$$\boldsymbol{\Lambda}_{\mathrm{R}}(t) \equiv (\tilde{\alpha}\cos_{\mathrm{R}}(\Omega t), -\tilde{\alpha}\sin_{\mathrm{R}}(\Omega t), 0)\,, \tag{55}$$

which is based on a 2π-periodic ramp (R) or symmetrical triangular wave function

$$\begin{aligned} \sin_{\mathrm{R}}(x) &\equiv \left\{\tfrac{\pi(-1)^m}{4}(x - m\pi)\,,\ \text{for } -\tfrac{\pi}{2} \le x - m\pi < \tfrac{\pi}{2}\right. \\ &= \sum_{n>0,\mathrm{odd}} \frac{(-1)^{\frac{n-1}{2}}}{n^2}\sin(nx), \qquad (56\mathrm{a}) \\ \cos_{\mathrm{R}}(x) &\equiv \sin_{\mathrm{R}}(x + \pi/2). \qquad (56\mathrm{b}) \end{aligned}$$

With this choice— notice that $\cos_{\mathrm{R}}(n\pi) = (-1)^n\pi^2/8$—, the contributions at frequencies $\pm\Omega$ are identical to those for IR case with Fourier amplitudes $\hat{H}^{(\pm1)}_{\mathrm{e/h,R}} = \hat{H}^{(\pm1)}_{\mathrm{e/h}}$ given in Eq. (27). Higher frequency Fourier components are

$$\hat{H}^{(\mp n)}_{\mathrm{e,R}} = \hat{H}^{(\mp n)}_{\mathrm{h,R}} = \frac{(-1)^{\frac{n-1}{2}}}{n^2}\frac{\tilde{\alpha}}{\hbar}p_x\sigma_\pm, \tag{57}$$

with n are positive, odd integers. The R driving, hence, violates properties (i) and (iii) of the IR case.

So far we have considered three different types of driving $\boldsymbol{\Lambda}(t)$, without any static SOC component $\boldsymbol{\Lambda}^{(0)} = \alpha_0/\hbar\hat{n}_0$ (with strength α_0 and spin axis along direction $\hat{n}_0$). $\hat{n}_0$ can be either parallel or perpendicular to the plane defined by $\boldsymbol{\Lambda}(t)$. In the following, we focus on the case of dominating $\boldsymbol{\Lambda}(t)$ such that $\alpha_0 \sim 0.2\tilde{\alpha}$ (nothing particular is expected for $\alpha_0 \gg \tilde{\alpha}$ since the system behaves, essentially, as a non-topological wire with static SOC and vanishing magnetic field). In Table I we define the labels used to identify 9 different situations addressed numerically with the method discussed in Sec. III A. Notice that drivings L and R, together with most cases with nonvanishing $\boldsymbol{\Lambda}^{(0)}$, cannot be easily mapped to a static model as in the IR case.

The results are presented in Fig. 4. At the critical point $\Omega = \Omega_{\mathrm{c}}$, the Floquet-band gaps close at $\varepsilon = \varepsilon_{0,0}(\Omega_{\mathrm{c}}) = \hbar\Omega_{\mathrm{c}}/2$ for $k \to 0$. For L driving, as in the IR case, Floquet-band gap (at small k) closes for the critical frequency forming Dirac-like cones. However, the bands are double degenerated and protected edge states are not favored: in a finite system two edge states would actually appear at each edge, but subject to a strong mixing by local perturbations. Here even in absence

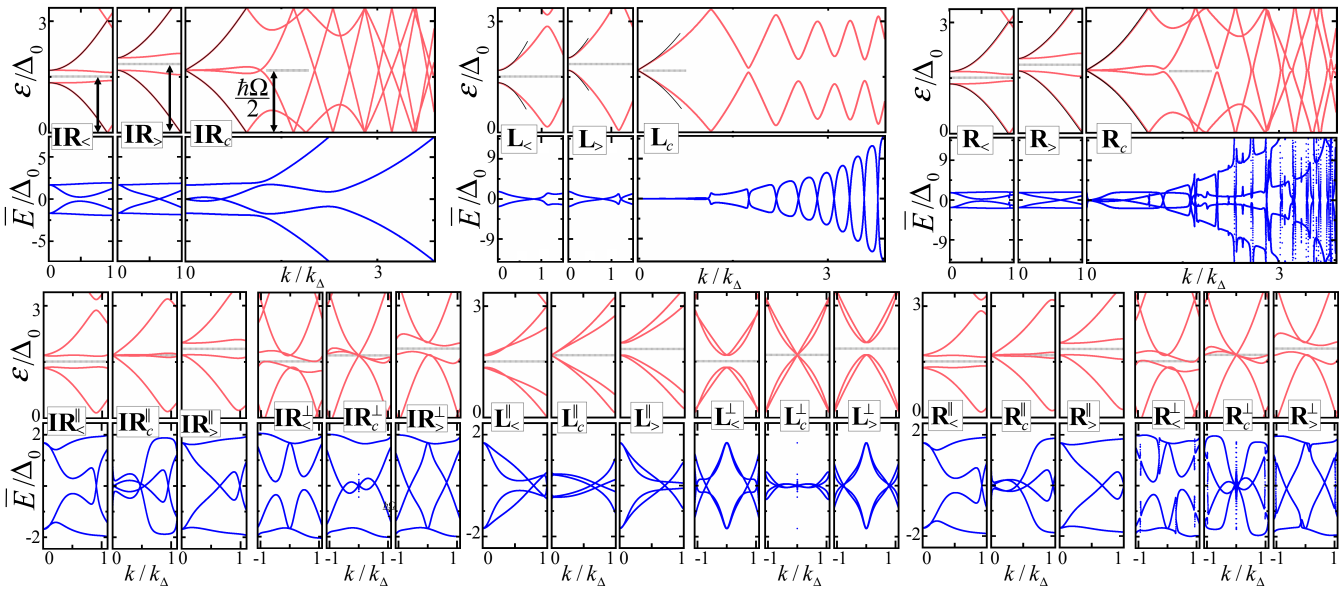

FIG. 4. Summary of results for the situations listed in Table I with $\mu = 1.35\Delta_0$, $\hbar\Omega_c \approx 3.36\Delta_0$, and $\tilde{E}_{so} = \tilde{\alpha}^2 m^*/(2\hbar^2) = 0.75\Delta_0$. Whenever present (lower panels), the static SOC component is set $\alpha_0 = \tilde{\alpha}/5$. Labels subindeces "<", "c" and ">" stand for Ω = $0.9\Omega_c$, Ω_c, and $1.1\Omega_c$, respectively. Floquet quasienergies are shown from 0 to $\hbar\Omega_c$. Floquet bands are symmetrical with respect to $\varepsilon = \hbar\Omega/2$ (horizontal grey line). We do not show the $-k$ quasienergies and mean energies whenever they are identical to the $+k$ ones. This is not the case for finite static SOC orthogonal to the periodic SOC driving. For vanishing static SOC (upper panels), solid black lines depict IR-quasienergy Floquet solutions— in particular, the bands associated to the topological transition [quasienergies from Eq.(33) with $n = 0$ generated by the energies of the static problem $E_{+,-}(k)$ and $E_{-,+}(k)$ given in Eq.(31)]. For L driving, the solutions with $\alpha_0 = 0$ are doubly degenerated. For R driving, higher-frequency driving components generate new transitions. Floquet transitions introduce avoided crossings in the quasienergy spectrum and strong discontinuities in the mean energies.[51,52] See text for further discussion.

of perturbations the localized states do not appear because those states mix each other. For completeness, in Fig.4 we also present results for the L driving coexisting with a static SOC where the referred double degeneracy is lifted. However, we have checked that no edge states can be found in the associated finite system (Sec.III B). This is something expected as we find two Floquet bands with finite slope closing the gap at the critical frequency.

For R driving, in the vicinity of $k = 0$ the Floquet bands are similar to those for the IR case, except at the critical frequency where a second pair of bands with flat dispersion also close. For larger k, the effect of higher harmonics modifies significantly the shape of quasienergy bands. The avoided crossings in quasienergy produce abrupt changes in the mean energies, the spikes in mean energies grow the larger the amplitude of the excitation.[51,52] In Sec. III B we show that related finite systems can hosts Majorana solutions at the edges, but presenting some signatures of the higher harmonics. Considering that the amplitudes of the R-driving Fourier components (Eq.(57)) decay very fast, these results suggest that Majorana fermions at the edges might be absent for arbitrary SOC drivings with significant contributions from higher harmonics.

TABLE I. Labels used to identify different SOC drivings $\boldsymbol{\Lambda}(t)$ in the presence of a static SOC component $\boldsymbol{\Lambda}^{(0)}$.

$\boldsymbol{\Lambda}^{(0)}$ \ $\boldsymbol{\Lambda}(t)$	$\boldsymbol{\Lambda}_{\mathrm{IR}}(t)$	$\boldsymbol{\Lambda}_{\mathrm{R}}(t)$	$\boldsymbol{\Lambda}_{\mathrm{L}}(t)$
$\boldsymbol{\Lambda}^{(0)} = \mathbf{0}$	IR	R	L
$\boldsymbol{\Lambda}^{(0)} \parallel \boldsymbol{\Lambda}(t)$	IR$^{\parallel}$	R$^{\parallel}$	L$^{\parallel}$
$\boldsymbol{\Lambda}^{(0)} \perp \boldsymbol{\Lambda}(t)$	IR$^{\perp}$	R$^{\perp}$	L$^{\perp}$

Finally, we briefly discuss the effect of a static SOC component with results shown in Fig. 4. For both IR and R driving, a $\boldsymbol{\Lambda}^{(0)}$ orthogonal to the plane defined by the driven SOC axis produces a breaking of $\pm k$ symmetry. Despite symmetry breaking, the main features discussed for vanishing $\boldsymbol{\Lambda}^{(0)}$ are maintained. This is related to the fact that the IR-mapping $\hat{U}^{\dagger}_{\mathrm{R}}(t)$ leads to static model of Ref. 6 except for a small SOC component along the magnetic field axis.

Besides, for parallel IR driving, closing Floquet bands at critical frequency show a tendency to reduce their mean energy. Moreover, the presence of Majorana states in corresponding finite systems is discouraged (see Sec. III B) whereas the orthogonal IR driving shows bounded MF undisturbed as those for $\alpha_0 = 0$.

B. Finite systems: Floquet Majorana Fermions

The Floquet Majorana fermions expected for this system have the form given in Eq. (36) with quasienergy $\varepsilon_{\mathrm{FMF}} = \varepsilon_{0,n}(\Omega) = (n + 1/2)\hbar\Omega$. Its linear dependence on the driving frequency determines that the mean energy of FMFs is zero, see Eq. (23). In the following, we apply a numerical method looking for solutions satisfying $\varepsilon \approx \varepsilon_{0,n}(\Omega)$ and $\overline{E} \approx 0$ in finite systems subject to a variety of drivings. Our numerical approach solves the eigenvalue problem for the evolution operator over a driving period, obtaining the quasienergies based on Eq.(18). As the evolution operator is evaluated from $t=0$ to $t = T$, its eigenvectors are the instantaneous form of the Floquet states at $t=0$.

We compute the evolution operator by dividing the period T in 120 time slices during which the driving is assumed to be constant. Due to the finite sample size, the system must be treated in real space: we use the customary finite-differences passage from the continuos to a tight-binding model with N sites. The wavefunction at each site is represented by a Nambu spinor and the pairing potential enters as an on-site coupling between the electron and hole sectors. The evolution operator becomes a $4N \times 4N$ matrix, $\hat{U}_T(t)$. The lattice spacing a_0 is chosen sufficiently small to turn the kinetic term [second order spatial derivative, now a hopping $t_\mathrm{h} = \hbar^2/(2m^* a_0^2)$ between neighbor lattice sites] into the largest energy scale in the system. The SOC [proportional to first-order spatial derivatives] leads to nontrivial spin-hopping terms with amplitudes given by the components of the vector $\left(\mathbf{\Lambda}(t) + \mathbf{\Lambda}^{(0)}\right)/(2a_0)$. As usual, the tight-binding model has the flexibility to deal with any site-dependent perturbation as local disorder or inhomogeneous driving, both discussed in Figs. 5 and 6.

We start by studying a clean, finite sample subject to IR driving in the supercritical regime $\Omega > \Omega_\mathrm{c}$. Bound states at the edges are expected as a result of change in topology, this is because the vacuum is in the trivial phase: it can be interpreted as having a large and negative chemical potential and therefore the critical frequency becomes larger than the driving frequency, $\hbar\Omega < 2\sqrt{\mu_\mathrm{vac}^2 + \Delta_0^2}$. In Fig. 5(a) we show the resulting quasienergies and mean energies. We sort the solutions according to growing quasienergies (left panel) or to growing mean energies (right panel), finding two solutions which are close to the Majorana conditions

$$\varepsilon = \varepsilon_{0,n}(\Omega)\,, \quad \overline{E} = 0. \tag{58}$$

We call these solutions $|a\rangle$ and $|b\rangle$, both found to have probability weight at the two edges. Similar features are found in Ref. 6 when calculating the eigenstates of finite, static systems. These eigenstates are bonding and antibonding combinations of Majorana fermions at the edges produced by finite size effects. The eigenenergies $\pm\delta E$ small but different from zero. To get rid of the mixing we should undo the (anti)bonding as[53]

$$\left|\phi_\pm^T(t=0)\right\rangle = \frac{1}{\sqrt{2}}\left(|a\rangle \pm |b\rangle\right). \tag{59}$$

In this way (see Fig.5(b)) we obtain two independent Floquet solutions, $\left|\phi_+^T(t=0)\right\rangle$ and $\left|\phi_-^T(t=0)\right\rangle$, one on each sample's edge. These are the solutions actually expected on long samples where the overlap between localized states is exponentially small.

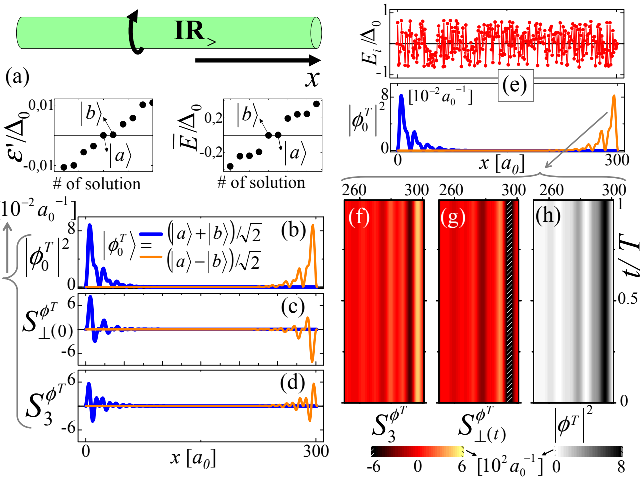

FIG. 5. Floquet Majorana states in a finite sample subject to the IR excitation in the $\Omega > \Omega_\mathrm{c}$ phase with $\tilde{E}_\mathrm{so} = \tilde{\alpha}^2 m^*/(2\hbar^2) = 0.5\Delta_0$. Reference quantities are Δ_0 and the wavelength $\lambda_\Delta = 2\pi/k_\Delta$, with $k_\Delta = \sqrt{2m^*\Delta_0}/\hbar$. The lattice spacing is $a_0 = 0.0225\lambda_\Delta$ (see text) with sample length $300a_0 = 6.75\lambda_\Delta$. We choose $\mu = 2\Delta_0$ such that $\hbar\Omega_\mathrm{c} = 2\sqrt{5}\Delta_0$, with driving frequency $\Omega = 1.15\Omega_\mathrm{c}$. (a) Floquet solutions ordered by growing quasienergy (left) and mean energy (right) . We plot $\varepsilon' \equiv \varepsilon - \hbar\Omega/2$ for $0 \leq \varepsilon \leq \hbar\Omega$. Two edge states, $|a\rangle$ and $|b\rangle$, are found with $\varepsilon \approx \hbar\Omega/2$ and mean energy $\overline{E} \approx 0$. Isolated Floquet Majorana fermions at each edge, $\left|\phi^T\right\rangle$, are extracted from the bonding and antibonding combinations of $|a\rangle$ and $|b\rangle$ (see text). For the two FMF states at $t=0$ we plot, as a function of the position x: (b) the probability density, $|\phi_0^T|^2 \equiv |\phi^T(x, t=0)|^2$; (c) the spin density along $\sigma_{\perp(0)} = \sigma_2$, $S_{\perp(0)}^{\phi_0^T} \equiv S_{\perp(t)}^{\phi^T}(x, t=0)$; and (d) the spin density along σ_3, $S_3^{\phi_0^T} \equiv S_3^{\phi^T}(x, t=0)$. The spin density along $\sigma_{\parallel(0)} = \sigma_1$ (not shown) is zero. (e) We include uncorrelated disorder $E_i \in [-0.75\Delta_0, 0.75\Delta_0]$. FMF are found with probability density similar to that of clean systems shown in (b). FMF densities are plotted as a function of time along one driving period in the presence of disorder: (f) $|\phi^T(x,t)|^2$, (g) $S_{\perp(t)}^{\phi^T}(x,t)$, and (h) $S_3^{\phi^T}(x,t)$. The in-plane spin component rotates while the FMF state conserves its location (see text).

For studying the structure of the these solutions we first introduce the electron-hole identity and Pauli matrices τ_j with $j = 0, 1, 2, 3$. In this way, the operators in the 4-dimensional Nambu space can be written as a combination of the operators

$$\tau_j\sigma_i \equiv \begin{pmatrix} \tau_{j,11}\sigma_i & \tau_{j,12}\sigma_i \\ \tau_{j,21}\sigma_i & \tau_{j,22}\sigma_i \end{pmatrix}, \tag{60}$$

where $\tau_{j,\gamma\delta}$ $(\gamma, \delta = 1, 2)$ are the components of the τ_j matrix such that $\tau_{j,\gamma\delta}\sigma_i$ are 2×2 blocks operating on spin space. The components $\{1, 2, 3, 4\}$ in the Nambu space are associated to $\tau\sigma = \{++, +-, -+, --\}$, respectively, where τ and σ refer to the ± 1 eigenvalues of τ_3 and σ_3. Notice that the combination $\tau_e \equiv (\tau_0 + \tau_3)/2$ $[\tau_h \equiv (\tau_0 - \tau_3)/2]$ has one single nonzero element, $\tau_{e,11} = 1$ $[\tau_{h,22} = 1]$, and it is useful for writing operators associated to the electron [hole] sector only.

For the time-dependent solution $\left|\phi(t)\right\rangle = \mathrm{e}^{-\frac{\mathrm{i}}{\hbar}\varepsilon t}\left|\phi^T(t)\right\rangle$ we define the instantaneous probability density $|\phi^T(x,t)|^2$ as the sum of the electron and hole probability densities of the associated Floquet state, $\rho_{e/h}^{\phi^T}(x,t)$. These are obtained when computing the expectation value of the identity operator $\hat{\mathbf{1}} \equiv$

$\int dx\,|x\rangle\langle x|\,(\tau_e+\tau_h)\sigma_0$:

$$\langle\phi(t)|\,\hat{\mathbf{1}}\,|\phi(t)\rangle = \int_{-\infty}^{\infty} dx \left(\rho_e^{\phi^T}(x,t) + \rho_h^{\phi^T}(x,t)\right),$$
$$\rho_{e/h}^{\phi^T}(x,t) \equiv \sum_{\sigma,\tau,\tau'} \left\langle \phi^T(t) \middle| x\tau\sigma \right\rangle \langle\tau|\tau_{e/h}|\tau'\rangle \left\langle x\tau'\sigma \middle| \phi^T(t) \right\rangle. \quad (61)$$

Similarly, related spin densities also evolve in time. The total spin density, $S_{i,\mathrm{tot}}^{\phi^T}(x,t)$, is the sum of the electron and holes probability densities in the associated Floquet state: $S_{i,e/h}^{\phi^T}(x,t)$. These are obtained by computing the expectation value of $\hat{S}_i \equiv \int dx\,|x\rangle\langle x|\,(\tau_e+\tau_h)\sigma_i$, with $i=1,2,3$ ($\hbar/2$ factors skipped for simplicity):

$$\langle\phi(t)|\,\hat{S}_i\,|\phi(t)\rangle = \int_{-\infty}^{\infty} dx \left(S_{i,e}^{\phi^T}(x,t) + S_{i,h}^{\phi^T}(x,t)\right), \quad (62)$$
$$S_{i,e/h}^{\phi^T}(x,t) \equiv \sum_{\sigma,\sigma',\tau,\tau'} \left\langle \phi^T(t) \middle| x\tau\sigma \right\rangle \langle\sigma,\tau|\tau_{e/h}\sigma_i|\sigma',\tau'\rangle \left\langle x\tau'\sigma \middle| \phi^T(t) \right\rangle.$$

Notice that the densities defined in Eq.(61) and Eq.(62) are properties of the physical state because the quasienergy phase factor cancels out. Moreover, due to such cancelation the resulting densities are the same irrespective of which shifted version of the Floquet state (see Eq.(19)) is taken.

As mentioned above, the states $\left|\phi_{\pm}^T(t)\right\rangle$ studied in this section [constructed with Eq.(59)] satisfy (numerically) the Majorana condition of Eq.(58). From hereon, we use $\left|\phi^T(t)\right\rangle$ to refer to any of these two states. In all presented situations (Figs. 5 and 6) we find $|\phi^T(x,t)|^2/2 = \rho_e^{\phi^T}(x,0) = \rho_h^{\phi^T}(x,0)$ and $S_{i,tot}^{\phi^T}(x,0) = 0$ for all i = 1, 2 and 3, namely, $S_{i,e}^{\phi^T}(x,0) = -S_{i,h}^{\phi^T}(x,0)$. Notice this differs from the regular type of quasiparticle states arising in an s-wave spin-degenerated BdG Hamiltonian; the latter cannot have vanishing $S_{i,tot}^{\phi}(x,0)$ for all three spin directions simultaneously. However, the result coincides with what is expected for a Majorana fermion as its own antiparticle (see Nambu-space representation of Eq.(36)). In what follows, we focus in the spin densities for electrons $S_i^{\phi^T}(x,t) \equiv S_{i,e}^{\phi^T}(x,t)$ as it is meaningless to discuss the total spin of a Majorana solution.

In Fig.5, for both clean and disordered systems subject to IR driving in the $\Omega > \Omega_c$ phase, we present the total probability density $|\phi^T(x,t)|^2$ and the electron spin densities. In Fig.5(d) we see that the states at different edges have the same $S_3^{\phi^T}(x,0)$ profile. Moreover, these profiles do not change with time as shown in Fig.5(f). This is equivalent to what found for the electron spin density along the magnetic-field axis for MF in the static system of Ref. 6 (where the larger the SOC in relation to the Zeeman energy, the smaller this component[54]). In our non-magnetic system, the associated direction is normal to the plane defined by the IR driving, see Eq.(14).

Additionally, in Fig.5(c) we see that the FMF solutions have opposite electron spin in-plane components which change as a function of time as shown in Fig. 5(g). We have defined the parallel, $\sigma_{\|(t)}$, and the perpendicular, $\sigma_{\perp(t)}$, spin directions with respect to the *instantaneous* SOC axis $\mathbf{\Lambda}_{\mathrm{IR}}(t)$:

$$\sigma_{\|(t)} \equiv \sigma_1\cos(\Omega t) - \sigma_2\sin(\Omega t), \quad (63a)$$
$$\sigma_{\perp(t)} \equiv \sigma_2\cos(\Omega t) + \sigma_1\sin(\Omega t). \quad (63b)$$

We find that the spin density $S_{\|(t)}^{\phi^T}(x,t)$ is zero (not shown) while $S_{\perp(t)}^{\phi^T}(x,t)$ in Fig.5(d) remains constant. This indicates that the in-plane electron spin components rotate as a function of time. This rotation is already expected from Eq. (36) as a mapping of the spin properties of MFs present in the static system of Ref. 6, which show a finite electron spin density *normal* to both the SOC axis and the magnetic-field axis. Such spin component assumes opposite signs for MFs located at opposite edges of the sample,[54] in agreement with our results entirely obtained within the periodically driven system.

Figure 5(e) presents one realization of uncorrelated disorder incorporated in all remaining results of this section, including time-evolved properties of Floquet states depicted in Figs. 5(f), 5(g) and 5(h). The disorder is implemented as tight-binding onsite energy fluctuations $E_i \in [-0.75\Delta_0, 0.75\Delta_0]$ chosen from an uniform distribution. Its characteristic energy is comprable to Δ_0 and larger than the SOC-driving energy scale excitation, $\tilde{E}_{\mathrm{so}}$. We have deliberately used short-range disorder in order to avoid that long sections of homogeneous disturbances drive parts of the system outside of the topological phase to be characterized. The robustness of the results to disorder is a signature of their topological origin.

Figure 6 shows several situations alternative to the IR driving including disorder. There we plot the probability densities for the states $\left|\phi^T(t)\right\rangle$ at $t = 0$ for a supercritical driving frequency $\Omega = 1.15\Omega_c$. The Fig.6(a) presents results for R driving. Localized states at edges have different profiles due to the presence of higher harmonics, evolving as a function of time in contrast to IR driving (not shown).

Systems subject to L driving (not shown) do not present Floquet states satisfying the Majorana conditions of Eq. (58). This is due to the double degeneracy of Floquet states, inconsistent with topologically protected unpaired edge states. Similarly, the presence of partial L driving tends to delocalize Majorana states. In Fig.6(b) we show a system subject to hybrid IR/L drivings on the left and right of the sample, respectively. We find that one of the states is localized on left edge while the partner is delocalized all over the sample. The presence of IR driving introduces Majorana-like solutions but only one of them is localized at the edge because of the L driving.

Figures 6(c) and 6(d) show results for IR driving in the presence of an small static SOC component, both parallel and orthogonal to the plane defined by the driving, respectively. In either case, localized Majorana solutions similar to those for the pure IR case are found at the sample edges. The orthogonal configuration is less affected by the static SOC, presenting a highly symmetric state distribution in contrast to the parallel configuration. This is consistent with the behavior of the mean energies (cases $\mathrm{IR}^{\|}$ and $\mathrm{IR}^{\perp}$ in Fig.4) for extended solutions with small k.

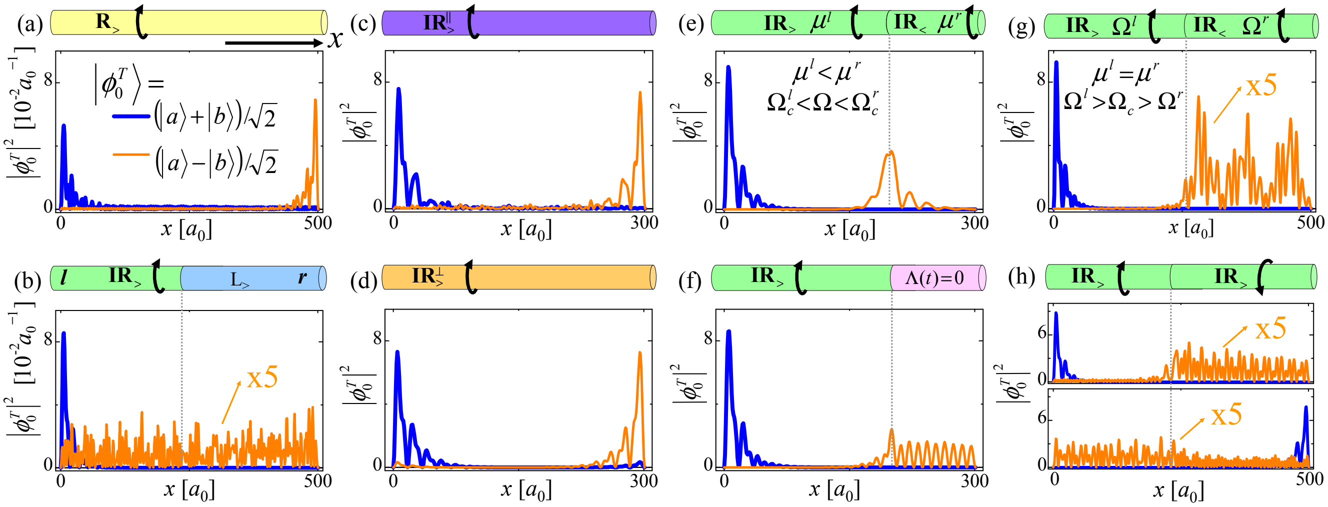

FIG. 6. Floquet Majorana states in finite samples subject to different types of SOC drivings and/or static SOC. All samples include disorder as the one given in Fig. 5(e). Unless otherwise stated the parameters a_0, μ, Ω_c, $\Omega = 1.15\Omega_c$ and $\tilde{E}_{so}$ are those given in Fig. 5. As in Fig.5, decoupled solutions are obtained by combining Floquet states $|a\rangle$ and $|b\rangle$ with $\varepsilon \approx \hbar\Omega/2$ and $\overline{E} \approx 0$. In all cases we plot the probability density $|\phi_0^T|^2 \equiv |\phi^T(x, t=0)|^2$ of the two (or more) FMF candidate states. We rescale some curves (×5) to improve visibility. (a) Full sample with R driving. (b) Left (l) section of the sample is subject to IR driving whereas the right section (r) is L-driven. (c)-(d) IR-driven sample in the presence of a static SOC with $\alpha_0 = 0.2\tilde{\alpha}$ either parallel (c) or perpendicular (d) to the plane of the IR driving. (e) IR-driven sample with inhomogeneous chemical potential on the left and right sections, $\mu^l = 2\Delta_0 = \mu^r/2$. The driving frequency is $1.15\Omega_c^l$ but smaller than the Ω_c^r. (f) IR-driven sample on the left section in contact with no SOC on the right. (g) IR-driven sample subject to different driving frequencies on left and right sections, $\Omega_l = 2\Omega_r = 1.15\Omega_c$: the left (right) section is in the supercritical (subcritical) regime. (h) Sample subject to counterrotating IR drivings with $\Omega = 1.15\Omega_c$, clockwise (counterclokwise) on the left (right) section of the sample. Four Floquet states arise in this case.

In Fig.6(e) we present the results for IR driving with inhomogeneous chemical potential. The driving frequency is chosen to supercritical on the left and subcritical on the right. Majorana states are found at the edges of the left section. This is in full agreement with what expected by virtue of the mapping to the static topological system of Ref. 6.

In Fig.6(f) we show the Floquet Majorana states for the case in which the left section is subject to IR driving ($\Omega > \Omega_c$) while the right part is free of any SOC. We find two Majorana states at the edges of the left section, this time with one delocalized solution penetrating into the right section. This is expected, indeed, since the section with vanishing SOC maps, using the time-dependent spin rotation for the whole system, into a static superconductor in which the Zeeman energy is *larger* than Δ_0, leading to $E = 0$ solutions that are not gapped because the SOC is zero.

In Fig. 6(g) we have investigated a situation in which the sample is subject to inhomogeneous IR-driving frequencies: Ω^r on the right section and $\Omega^l = 2\Omega^r$ on the left one. We choose a supercritical $\Omega^l = 1.15\Omega_c$ such that Ω^r is subcritical. We avoid dealing with incommensurable frequencies so that our choice allows for the application of the Floquet theorem. The results are similar to the case of Fig. 6(f), with a localized Majorana solution on the left and a delocalized state penetrating into the right section.

Finally, we obtained the Floquet solutions for counterrotating IR drivings: clockwise rotation on the left section and counterclockwise on the right one, see Fig. 6(h). The situation results interesting since both sides satisfy the supercritical condition $\Omega > \Omega_c$. As in all other cases, we have chosen the position of the left/right interface away from the geometrical center of the sample to avoid solutions influenced by symmetry. We find two pairs of states satisfying the Majorana condition. The finite-size offsets to Eq.(58), $\pm\delta\varepsilon$ and $\pm\delta\overline{E}$, are different for the two pairs. For each pair we find a localized FMF at one edge and a delocalized solution over the opposite side of the sample.

The results discussed along this section, obtained in the presence of disorder, confirms the existence of bounded Floquet states at the edges systems subject to IR driving. They are Floquet Majorana fermions arising in absence of magnetic fields when the driving frequency is sufficiently large. When the samples are enlarged, the local probability density of the delocalized FMF solutions decrease [see Figs. 6(b), 6(f), 6(g), and 6(h)] whereas the localized solutions remain unaffected.

IV. CONCLUSIONS

Starting from a well-known quantum system hosting Majorana fermions for sufficiently large magnetic fields, we derived a non-magnetic scheme sharing such properties thanks to periodic driving. Our proposal disregards Zeeman coupling: its role is played by the driving frequency of a rotating spin-orbit coupling axis. An effective breaking of time reversal symmetry is induced by the definite rotation sense (either clockwise or counterclockwise). Otherwise, double degeneracy (due to a time-reversal symmetry) would discourage the appearance of a single Majorana solution at the sample's edges. A experimental realization of this theoretical model would require the ability to control the SOC axis as a function of time. This can be envisioned in systems with lateral gates in orthogonal directions that modulates the symmetry of the quantum well containing a superconducting electron system. Alternatively, in cold-atom quantum wires the Rashba coupling could be engineered to change its axis with time.[9,55] The proposal incorporates the virtue of being a non-magnetic platform for Majorana fermions into the active field of Floquet topological matter.[9,18,21,24–27]

Our mapping allows analytical treatment in the case of ideal rotating (IR) driving. For supercritical driving frequency $\Omega > \Omega_c$, i.e., in the Floquet topological superconducting phase, Floquet Majorana fermions are found at the edges of finite samples. While in static systems Majorana fermions appear at zero energy, the FMFs here have quasienergy $\hbar\Omega\,(n + 1/2)$. We point out that these FMFs, as those reported in Ref. 9 having quasienergy linear in Ω, have *zero mean energy*. This fact can be important on the light of Ref. 38, where Arimondo et al. provide experimental and theoretical indications that the mean-energy variable— once the memory of the initial condition is lost— might play a key role in dictating the occupancy of Floquet states.[39] As the chemical potential lies at zero energy, this might determine that, at zero temperature, the reported FMFs are the *highest mean-energy* occupied Floquet states.

We have also investigated different types of drivings based on time-dependent SOC. Rotating SOC drivings are needed because of the requirement of time-reversal-symmetry breaking. For non-ideal SOC rotations the numerical results show that higher harmonics can degrade the formation of FMFs. Similar degradation is found in the case of an IR driving coexisting with a static component of SOC contained in the plane of the rotation. We demonstrate the great deal of possibilities for FMFs at edges and interfaces by exploring only a handful of examples.

For finite samples, our numerical simulations show that the FMFs appear even in the presence of disorder. This is remarkable, considering that FMFs in a finite sample are not protected by a gap in quasienergy. In the case of IR driving, numerical results can be understood analytically by a mapping to the static model, noticing that static disorder maps trivially: Majorana fermions in those systems are robust to disorder smaller than the protecting energy gap. Interestingly, an underlying "gap", which is not visualized straightforwardly from the Floquet quasienergy spectrum, is protecting the FMFs in these driven systems.

Finally, we expect that tunneling probing (with a normal lead) of the edge of a sample in the Floquet TSP phase will lead to observe two peaks in the differential conductance dI/dV at bias voltages $V_\pm = \pm\hbar\Omega/2$. Those peaks have different heights dictated by the ratio between the effective Zeeman energy and the spin-orbit coupling strength. The peaks are not present in the trivial phase ($\Omega < \Omega_c$) and a background with structure is visible in both phases (including pumping effects,[56–58] as current for zero bias due to the rotating-SOC). These qualitative conclusions are obtained within a picture that makes use of the rotating frame transformation [the driven part of the sample is mapped to the static topological phase, having an unpaired MF at its edge at $E = 0$] and shifts the Fermi energies in the normal probe differently for electrons with spin $\sigma_z = \pm$: an energy $\sigma_z\hbar\Omega/2$.[59] The mentioned shifts in the Fermi occupations are introduced to conserve the number of electrons in the static lead before and after the transformation (notice that the effective magnetic field splits the *up* and *down* bands) as the ultimate goal is computing transport from the lead to other parts of the system.[60]

Certainly, among future directions of study appears a quantitative determination of the mentioned observable signatures (and others) to detect the Floquet TSP. Results beyond the IR case would requiere a Floquet-Keldysh approach,[21,61,62] which here becomes non-standard because the superconducting 1D lead has a time-dependent spin-orbit coupling. Other line includes developing schemes to use the localized Floquet Majorana fermions (the ones reported here or those reported in Ref.9) for quantum information purposes: quantum memory, braiding, etc. Crucial in all cases appears having a better understanding of which of the Floquet states are occupied, a problem that falls within the complex subject of statistical mechanics for driven systems.[63,64] Here, we have pointed out that interesting intrinsic physical properties are expected if one develops the ability to manipulate the SOC axis as a function of time. Identifying candidate platforms in which such ability is achievable would be desirable and it certainly would motivate more research on this and other systems, this includes situations in absence of superconductivity.

ACKNOWLEDGMENTS

We acknowledge useful discussions with A. Doherty, K. Flensberg, A. Lobos and J. M. Taylor. AAR acknowledges support from the Australian Research Council Centre of Excellence scheme CE110001013, from ARO/IARPA project W911NF-10-1-0330, and the hospitality of University of Seville. DF acknowledges support from the Ramón y Cajal program, from the Spanish Ministry of Science and Innovation's projects No. FIS2008-05596 and FIS2011-29400, and from the Junta de Andalucía's Excellence Project No. P07-FQM-3037.

---

[1] L. Kouwenhoven, APS March Meeting (2012); R. F. Service, Science **332**, 193 (2011); M. Franz, Physics **3**, 24 (2010).

[2] V. Mourik, K. Zuo, S. M. Frolov, S. R. Plissard, E. P. A. M. Bakkers, and L. P. Kouwenhoven, Science **336**, 1003 (2012).

[3] L. P. Rokhinson, X. Liu, and J. K. Furdyna, ArXiv e-prints (2012), arXiv:1204.4212 [cond-mat.mes-hall].

[4] A. Das, Y. Ronen, Y. Most, Y. Oreg, M. Heiblum, and H. Shtrikman, ArXiv e-prints (2012), arXiv:1205.7073 [cond-mat.mes-

hall].

[5] L. Fu and C. L. Kane, Phys. Rev. Lett. **100**, 096407 (2008).

[6] J. D. Sau, R. M. Lutchyn, S. Tewari, and S. Das Sarma, Phys. Rev. Lett. **104**, 040502 (2010); J. Alicea, Phys. Rev. B **81**, 125318 (2010); Y. Oreg, G. Refael, and F. von Oppen, Phys. Rev. Lett. **105**, 177002 (2010).

[7] A. C. Potter and P. A. Lee, Phys. Rev. Lett. **105**, 227003 (2010).

[8] M. Sato, Y. Takahashi, and S. Fujimoto, Phys. Rev. Lett. **103**, 020401 (2009).

[9] L. Jiang, T. Kitagawa, J. Alicea, A. R. Akhmerov, D. Pekker, G. Refael, J. I. Cirac, E. Demler, M. D. Lukin, and P. Zoller, Phys. Rev. Lett. **106**, 220402 (2011).

[10] N. Read and D. Green, Phys. Rev. B **61**, 10267 (2000).

[11] A. Y. Kitaev, Physics-Uspekhi **44**, 131 (2001).

[12] In fact, the existence of helical edge modes in the topological insulating phase is also originated by SOC coupling, see for example Refs. 65 and 66.

[13] S. Sasaki, M. Kriener, K. Segawa, K. Yada, Y. Tanaka, M. Sato, and Y. Ando, Phys. Rev. Lett. **107**, 217001 (2011).

[14] D. A. Ivanov, Phys. Rev. Lett. **86**, 268 (2001).

[15] A. Stern, F. von Oppen, and E. Mariani, Phys. Rev. B **70**, 205338 (2004).

[16] C. Nayak, S. H. Simon, A. Stern, M. Freedman, and S. Das Sarma, Rev. Mod. Phys. **80**, 1083 (2008).

[17] J. Alicea, Y. Oreg, G. Refael, F. von Oppen, and M. P. A. Fisher, Nat Phys **7**, 412 (2011).

[18] T. Kitagawa, E. Berg, M. Rudner, and E. Demler, Phys. Rev. B **82**, 235114 (2010).

[19] T. Oka and H. Aoki, Phys. Rev. B **79**, 081406 (2009).

[20] P. H. Rivera, A. L. C. Pereira, and P. A. Schulz, Phys. Rev. B **79**, 205406 (2009).

[21] H. L. Calvo, H. M. Pastawski, S. Roche, and L. E. F. F. Torres, Applied Physics Letters **98**, 232103 (2011).

[22] Y. Zhou and M. W. Wu, Phys. Rev. B **83**, 245436 (2011).

[23] M. Busl, G. Platero, and A.-P. Jauho, Phys. Rev. B **85**, 155449 (2012).

[24] Z. Gu, H. A. Fertig, D. P. Arovas, and A. Auerbach, Phys. Rev. Lett. **107**, 216601 (2011).

[25] N. H. Lindner, G. Refael, and V. Galitski, Nat. Phys. **7**, 490 (2011); T. Kitagawa, M. S. Rudner, E. Berg, and E. Demler, Phys. Rev. A **82**, 033429 (2010).

[26] T. Kitagawa, M. A. Broome, A. Fedrizzi, M. S. Rudner, E. Berg, I. Kassal, A. Aspuru-Guzik, E. Demler, and A. G. White, Nat Commun **3**, 882 (2012).

[27] G. Liu, N. Hao, S.-L. Zhu, and W. M. Liu, ArXiv e-prints (2012), arXiv:1203.3848 [cond-mat.mes-hall].

[28] For time-independent unitary transformations the topological properties are common to the two linked Hamiltonians. For a general time-dependent unitary transformation the topological properties are not always preserved.

[29] B. Braunecker, G. I. Japaridze, J. Klinovaja, and D. Loss, Phys. Rev. B **82**, 045127 (2010).

[30] M. Kjaergaard, K. Wölms, and K. Flensberg, Phys. Rev. B **85**, 020503 (2012).

[31] D. Jaksch and P. Zoller, New Journal of Physics **5**, 56 (2003).

[32] E. J. Mueller, Phys. Rev. A **70**, 041603 (2004).

[33] A. S. Sørensen, E. Demler, and M. D. Lukin, Phys. Rev. Lett. **94**, 086803 (2005).

[34] Y.-J. Lin, R. L. Compton, K. Jimenez-Garcia, J. V. Porto, and I. B. Spielman, Nature **462**, 628 (2009).

[35] I. I. Rabi, Phys. Rev. **51**, 652 (1937).

[36] T. Kitagawa, T. Oka, A. Brataas, L. Fu, and E. Demler, Phys. Rev. B **84**, 235108 (2011).

[37] Solutions for small $k \neq 0$ form a Dirac cone that closes at zero mean energy but the two states at its vertex, $k = 0$, have finite mean energies, $\pm\Omega_c/2$.

[38] E. Arimondo, D. Ciampini, A. Eckardt, M. Holthaus, and O. Morsch, ArXiv e-prints (2012), arXiv:1203.1259 [cond-mat.quant-gas].

[39] H.-P. Breuer, W. Huber, and F. Petruccione, Phys. Rev. E **61**, 4883 (2000).

[40] P. G. de Gennes, *Superconductivity of Metals and Alloys* (W. A. Benjamin Inc. New York, 1966).

[41] X.-L. Qi and S.-C. Zhang, Rev. Mod. Phys. **83**, 1057 (2011).

[42] R. Jackiw and C. Rebbi, Phys. Rev. D **13**, 3398 (1976).

[43] M. Leijnse and K. Flensberg, ArXiv e-prints (2012), arXiv:1206.1736 [cond-mat.mes-hall].

[44] I. L. Aleiner and V. I. Fal'ko, Phys. Rev. Lett. **87**, 256801 (2001).

[45] D. Frustaglia and K. Richter, Foundations of Physics **31**, 399 (2001), 10.1023/A:1017550822221.

[46] M. Popp, D. Frustaglia, and K. Richter, Phys. Rev. B **68**, 041303 (2003).

[47] J. J. Sakurai, *Modern Quantum Mechanics (2nd Edition)* (Addison Wesley, 1994).

[48] A. G. Fainshtein, N. L. Manakov, and L. P. Rapoport, Journal of Physics B: Atomic and Molecular Physics **11**, 2561 (1978).

[49] T. Ando, Phys. Rev. B **40**, 5325 (1989).

[50] From Eq.(42) the difference between the mean energy of a Floquet state and the energy of the associated eigenstate in the static system is directly proportional to the expectation value of σ_z in the latter eigenstate.

[51] F. H. M. Faisal and J. Z. Kamiński, Phys. Rev. A **56**, 748 (1997).

[52] H. Hsu and L. E. Reichl, Phys. Rev. B **74**, 115406 (2006).

[53] An extra phase factor might be needed to decouple the two solutions, this depends on the direction of the SOC at $t = 0$ and/or on the arbitrary phases accompanying each of the computed eigenvectors.

[54] D. Sticlet, C. Bena, and P. Simon, Phys. Rev. Lett. **108**, 096802 (2012).

[55] C. Zhang, Phys. Rev. A **82**, 021607 (2010).

[56] M. Moskalets and M. Büttiker, Phys. Rev. B **66**, 205320 (2002).

[57] A. Brataas and Y. Tserkovnyak, Phys. Rev. Lett. **93**, 087201 (2004).

[58] L. Arrachea, Phys. Rev. B **72**, 125349 (2005).

[59] S.-H. Chen, C.-R. Chang, J. Q. Xiao, and B. K. Nikolić, Phys. Rev. B **79**, 054424 (2009).

[60] Notice that in this work we have applied the time-dependent unitary transformation of Eq.(11) to the states as a mathematical tool to obtain the solutions of the time-dependent BdG-Schroedinger equation dictated by $\hat{H}(t)$. In such mathematical framework the chemical potential μ appearing in $\hat{H}(t)$ is not modified at all when applying the transformation to the states.

[61] S. Kohler, J. Lehmann, and P. Hnggi, Physics Reports **406**, 379 (2005).

[62] F. Mahfouzi, J. Fabian, N. Nagaosa, and B. K. Nikolić, Phys. Rev. B **85**, 054406 (2012).

[63] D. W. Hone, R. Ketzmerick, and W. Kohn, Phys. Rev. E **79**, 051129 (2009).

[64] R. Ketzmerick and W. Wustmann, Phys. Rev. E **82**, 021114 (2010).

[65] C. L. Kane and E. J. Mele, Phys. Rev. Lett. **95**, 146802 (2005).

[66] S. Murakami, Phys. Rev. Lett. **97**, 236805 (2006).